Spectral Energy Distribution Fitting of the Bulge and Disk Components of Interacting Galaxies

by

Michael J.D. Palmer
B.Sc., Saint Mary's University, 2010

A Thesis Submitted in Partial Fulfillment of the
Requirements for the Degree of

MASTER OF SCIENCE

in the Department of Physics and Astronomy

Spectral Energy Distribution Fitting of the Bulge and Disk Components of Interacting Galaxies

by

Michael J.D. Palmer
B.Sc., Saint Mary's University, 2010

Supervisory Committee

Dr. Sara Ellison, Co-Supervisor
(Department of Physics & Astronomy)

Dr. Luc Simard, Co-Supervisor
(Department of Physics & Astronomy, National Research Council Canada)

Supervisory Committee

Dr. Sara Ellison, Co-Supervisor
(Department of Physics & Astronomy)

Dr. Luc Simard, Co-Supervisor
(Department of Physics & Astronomy, National Research Council Canada)

ABSTRACT

We perform spectral energy distribution fitting to the total integrated light, bulge and disk components of ≈ 650,000 spectroscopically selected galaxies from the sloan digital sky survey data release 7. Using 4-band photometry (u, g, r, i) we derive physical properties for these components with particular emphasis placed on the star formation rates (SFR) and stellar masses. Using the total integrated fits as an indicator of the goodness of fit, we show that reliable estimates of the SFR can be recovered using a specific SFR (sSFR) cut of log(sSFR /yr) ≥ -10.45. We construct a close pairs sample and match isolated controls based on stellar mass, z and local density for galaxies that pass the sSFR cut. We develop a method to cross correlate the pair galaxies' star formation rate posterior probability distribution functions (SFR PDFs) with the control SFR PDFs as a function of the pair galaxies projected separation, r_p. We show that the SFR of the close pair galaxies is enhanced relative to the control sample. The SFR enhancement is at a level of ≈ 0.25 dex above that of the control at the closest separations and declines to a plateau at ≈ 0.15 dex for separations of $30 < r_p < 60$ kpc/h. Between $60 < r_p < 80$ kpc/h there appears to be a slight increase in the enhancement to a level ≈ 0.25 dex above the control. It is suggested that we observe this increase, where other studies have failed to, based on the updated photometry provided by Simard et al. (2011). From our total pair sample we also select a subsample of galaxies that are classified as active galactic nuclei (AGN). We note that at close separations the pair AGN galaxies have enhanced SFRs relative to their matched controls. The SFR enhancement is largest at the smallest separations, reaching a level of ≈ 0.3 dex above the control. The SFR enhancement for the AGN pairs becomes consistent with their controls at projected separations of $20 < r_p < 80$ kpc/h. We construct a bulge and

disk pair sample that are required to pass the sSFR cut and match control bulges and disks, respectively, that also pass the sSFR cut. We cross correlate the bulge and disk pairs with their respective controls. We measure significant SFR enhancement in the bulge component of the interacting pairs. The SFR enhancement is highest at small separations, ≈ 0.4 dex, and steadily declines to ≈ 0.1 dex before turning around beyond $r_p > 50$ kpc/h to again reach a level ≈ 0.4 dex above the control bulges. The disk SFR enhancement is relatively flat beyond $r_p > 30$ kpc/h to a level ≈ 0.1 dex above the control and largely consistent with the control at close separations. The bulge and disk results suggest that the majority of induced star formation during an interaction is occurring in the bulge component, but that there is still slight SFR enhancement in the disk. We suggest that the upturn in the total and bulge SFR enhancement could potentially be caused by a delay between the interaction of the galaxy pairs and the onset of induced star formation.

Contents

List of Tables

List of Figures

ACKNOWLEDGEMENTS

First, I would like to thank Sara for giving me the opportunity to come to Victoria to work on this project and for guiding me along as it unfolded. Luc, I want thank you for all your insight and advice to help make this a great project. Thanks go out to Marcin as well, for your advice and help over the last 5 years.

Special thanks goes out to my personal postdoc Trevor. You've been a significant contributor to my Masters experience and it would not have been the same without you. Good luck at your next postdoc and in the future.

Thanks to office 408 for some great times! Hopefully I did not distract you to much! Good luck in the future and perhaps we shall cross paths again.

I want to thank my families. All of you were there for us when we were making some tough decisions and I hope I can continue to count on you.

Beedsie, none of this would have been possible without you there by my side. Thank you for putting up with me, for sticking with me and for saying yes!

DEDICATION

For family and friends. What's life without them?

Chapter 1

Introduction

Our current understanding of the universe is that structure is built hierarchically or bottom-up (e.g. White & Rees, 1978). A necessary consequence of this bottom-up scenario is that mergers will play a role in the formation and evolution of galaxies. Therefore, it is important for us to develop a better understanding of the physical processes occurring during galaxy mergers in order to better constrain galaxy evolution.

1.1 Mergers - Simulations

Using numerical simulations we have the ability to track individual mergers through cosmological timescales that are unfeasible through observations alone and to also help interpret what happens during galaxy - galaxy interactions. A key feature of these simulated interacting galaxies is the ability to determine the effect that the interaction has on the gas and existing stars in the two galaxies. Early simulations, such as the ones performed by Toomre & Toomre (1972) laid the ground work for future numerical simulations, successfully reproducing the tidal features seen in interacting galaxies, such as rings or tidal arms. However, these early simulations did not include all the necessary physics needed to account for what is physically occurring during mergers, such as the inflow of gas to the central regions of the interacting galaxies.

The works of Mihos & Hernquist (1994, 1996) looked at both major (galaxies of a similar mass) and minor (all other mass ratios) simulations and were able to track the flow of both stars and gas. They found that a changing gravitational potential, induced by a merger or an interaction, has the ability to drive available gas towards the centres of these galaxies. The reason that the gas funnels towards the centre of their galaxies is due to the

changing gravitational potential, i.e. bar formation, which in turn causes torques on the gas (e.g Barnes & Hernquist, 1996; Mihos & Hernquist, 1996). As the gas is torqued it loses some of its angular momentum and begins to fall towards the centre of the potential. The Kennicutt-Schmidt relation links gas density and star formation rate (SFR) (Schmidt, 1959; Kennicutt, 1989). Simulations of galaxies generally use an adopted form of this relation to derive SFRs for the galaxies. The funnelling of gas to the central regions of interacting galaxies causes the gas in the central regions to have a higher density than it would in an isolated non-interacting case. Using the Kennicutt-Schmidt relation, Mihos & Hernquist (1994, 1996) were able to show that for both major and minor mergers, there is a substantial burst of star formation induced by the buildup of gas in central regions of the interacting galaxies.

The magnitude of the induced SFR is dependent upon several different factors, with contributions coming from both the internal properties of the galaxies and the orbital parameters of the merger or interaction. The inclusion of a bulge component to an interacting disk galaxy has been shown to have an effect on the magnitude of induced star formation. The bulge is thought to stabilize the disk against a changing potential and prevent the inflow of gas during first passage, e.g. Mihos & Hernquist (1996). However, during coalescence, the gas that was previously unaffected by the interaction is then funnelled to the centre to fuel an intense starburst (e.g. Mihos & Hernquist, 1996; Cox et al., 2008).

In addition to the presence of a bulge playing a role on the magnitude of induced star formation, the orientation of the galaxy - galaxy interaction also plays a large part in determining the amount of induced star formation that is seen. As noted by, e.g. Mihos & Hernquist (1996) and Di Matteo et al. (2007), different orbital orientations can affect the magnitude of induced star formation. Both of these studies find that galaxy - galaxy interactions that have retrograde orbits produce a larger SFR enhancement. Mihos & Hernquist (1996) looked at one example of a prograde-retrograde interaction. They found that the increase of magnitude in enhanced SFR is due to increased shocks on the gas due to the different orbital parameters. The retrograde galaxy also accreted roughly 30% of the gas from the prograde galaxy. In addition, the prograde disk lost some of its available gas to its tidal tails causing the retrograde galaxy to have of order two times the amount of available gas to fuel a central starburst (Mihos & Hernquist, 1996). Di Matteo et al. (2007) looked at prograde-retrograde interactions in a more statistical sense, where they varied the morphology of the interacting galaxies and whether the galaxies merge or simply flyby one another without a final coalescence. They found that on average, the retrograde galaxies have a higher enhanced SFR than the prograde galaxies.

The role that the gas fraction, the fraction of a galaxy's total mass in gas, of the merging galaxies has on the SFR enhancement is still ambiguous. Di Matteo et al. (2007) found that for mergers, the gas fraction does not seem to be an important parameter in determining the maximum SFR induced by the merger event. Their result, spanned a wide range of different gas fractions and galaxy types, with no correlations noted. Contrary to the Di Matteo et al. (2007) result, both Perez et al. (2011) and Bournaud et al. (2011) find that the gas fraction plays an important role in mergers. In the Bournaud et al. (2011) simulations they show that high gas fraction mergers can lead to a factor of 10 higher SFR compared to isolated galaxies. The mass ratio between the merging galaxies has also been shown to have an effect on the level of SFR enhancement that is measured in simulations. Cox et al. (2008) looked at mergers between galaxies of varying mass, from 1:1 mass ratios up to 1:23. They found that the major mergers induced the largest burst of SFR and that the minor interactions did not have a significant effect, which is contrary to the works of Mihos & Hernquist (1994). Cox et al. (2008) attribute the differences in the results to changes and upgrades to the input physics used in the simulations. However, on a more galaxy by galaxy specific basis, Cox et al. (2008) found that the less massive minor companion galaxy had some levels of induced star formation that were hidden when looking at the global SFR, which is dominated by the more massive companion. The reason that the major mergers produced a larger burst of star formation is due to the mutual ability of both galaxies to tidally disturb each other and cause a significant amount of gas to funnel to the central regions. In the minor merger case the less massive galaxy is not massive enough to induce strong tidal effects on the more massive companion, Cox et al. (2008). Aside from inducing bursts of star formation, interactions and mergers are expected to have other interesting effects on the galaxies involved.

The newly formed reservoir of gas in the central regions of the interacting galaxy can accrete onto a central super massive black hole. Gas accretion onto a central super massive black hole is thought to deposit vast amounts of energy to the galaxy, turning on what is called an active galactic nucleus, AGN. The energy feedback from AGN is often appealed to as a mechanism to shut off ongoing star formation (e.g. Di Matteo et al., 2005) and to prevent an overabundance of high mass galaxies in simulations, e.g. Bower et al. (2006). As described above, there is induced star formation in these central regions of interacting galaxies. However, how does this induced star formation fit in with the presence of an AGN, which is used to eliminate star formation? Hopkins (2012) studied both the SFRs in mergers as well as the black hole accretion rate. They show that the peak SFR in a merger occurs a few tens to hundreds of million years before the peak in the black hole accretion

rate. The star formation is not immediately shut off when the accretion rate reaches its peak, rather it slowly declines, implying that AGN activity and induced star formation can occur concurrently.

The gas that is being funnelled towards the central component has also be shown to have an effect on the measured metallicity in these regions during simulations (e.g. Perez et al., 2006; Montuori et al., 2010; Rupke et al., 2010; Perez et al., 2011; Torrey et al., 2012). As an example, Torrey et al. (2012) simulated the metallicity distribution of galaxies undergoing interactions. The metal poor inflowing gas has the effect of lowering the metallicity in the nuclear region of their galaxies. However, this lowering of metallicity is not terminal; due to the known enhancement in star formation, the metallicity is raised due to the evolution of these newly formed stars and the ejection of their metals by supernova. Torrey et al. (2012) found that the combined effect of these two processes resulted, on average, in a decrease in the nuclear metallicity of interacting galaxies, followed by enhancement. The long term change in metallicity depends on the specific interaction and could lead to either lower or enhanced central metallicity.

The environment in which the interacting galaxies reside has also been shown to have an effect on galaxy properties. Tonnesen & Cen (2011) examined the specific SFR (SFR normalized by the stellar mass, sSFR) for $\approx$ 1000 simulated galaxies in a wide range of local densities. From densities consistent with voids up to and including densities of galaxy clusters. Tonnesen & Cen (2011) find that gravitationally bound pairs tend to have larger sSFRs compared to non-pair galaxies independent of their environment. However, as a function of local density, it is the high density regions that have a larger fraction of galaxies with enhanced sSFRs compared to non-pair galaxies. Tonnesen & Cen (2011) find that their results are opposite to what observations (see below) find and cite observational biases as being a potential candidate for the disagreement. They find that galaxies in the void, regardless of whether they're in a pair or not, have relatively large sSFRs. Comparatively, cluster galaxies on average have low sSFRs, where a sSFR enhancement in a cluster pair will then appear more significant than an enhancement in the void.

1.2 Mergers - Observations

Many of the features noted by merger simulations have been confirmed by observations. Early evidence of induced star formation was inferred from the colours of both "normal" and "peculiar" galaxies. Larson & Tinsley (1978) noted that there is a larger spread in colour - colour space for peculiar galaxies compared to normal galaxies. Using a suite of

models with declining SFRs, they attributed this spread of galaxy colours to differences in SFRs and the inclusion of bursts of star formation. More recently Bergvall et al. (2003); Ellison et al. (2010); Patton et al. (2011) looked at the colours of interacting galaxies compared to well-defined control samples. These studies noted that the central colours of the interacting galaxies were bluer compared to their controls. The bluer colours in the central regions of the interacting galaxies are believed to come from a younger population of stars that are present as a result of induced star formation.

Enhanced star formation rates have been observed in several studies, using various surveys, at low redshifts (e.g Barton et al., 2000; Bergvall et al., 2003; Lambas et al., 2003; Alonso et al., 2004, 2006; Woods & Geller, 2007; Ellison et al., 2008, 2010; Lambas et al., 2012; Alonso et al., 2012; Scudder et al., 2012) and high redshifts (e.g. Lin et al., 2007; Wong et al., 2011). One of the key features of these studies is the general agreement that the SFR enhancement depends upon the projected separations of the pair galaxies. The SFR enhancement is strongest when galaxies are at their closest separations and declines as the separation increases. Recently Scudder et al. (2012) found a "plateau" in the SFR enhancement out to wider separations (at least 80 kpc/h), implying that the pair galaxies are still significantly enhanced in SFR over their control galaxies. This effect was first seen in the colours of interacting galaxies by Patton et al. (2011). The cause of this plateau is believed to be due to a delay between the interaction of the galaxies and the onset of induced star formation, Scudder et al. (2012).

The magnitude of the measured SFR enhancement has been shown to depend upon several different factors. The SFR enhancement has been observed to depend upon the mass ratio of the galaxies involved, (e.g. Woods & Geller, 2007; Ellison et al., 2008; Scudder et al., 2012). There is general agreement between these studies that galaxies that are involved in a major merger (similar masses) have the largest enhanced SFRs. However, galaxies involved in minor mergers generally still exhibit some SFR enhancement relative to their controls. Ellison et al. (2008) found that there is still moderate SFR enhancement when all mass ratios are considered (their study was limited to $0.1 < \mathrm{Mass}_{host}/\mathrm{Mass}_{companion} < 10$) and Scudder et al. (2012) found significant SFR enhancement for minor galaxy interactions with $\mathrm{Mass}_{host}/\mathrm{Mass}_{companion} < 0.33$ and $\mathrm{Mass}_{host}/\mathrm{Mass}_{companion} > 3$, Figure 1.1. The environment in which pair galaxies reside has also been demonstrated to have an effect on the measured magnitude of SFR enhancement. It has been found that mergers that occur in low to intermediate density environments produce SFR enhancements of a greater magnitude than mergers that occur in high density environments (e.g. Alonso et al., 2004, 2006; Ellison et al., 2010; Alonso et al., 2012).

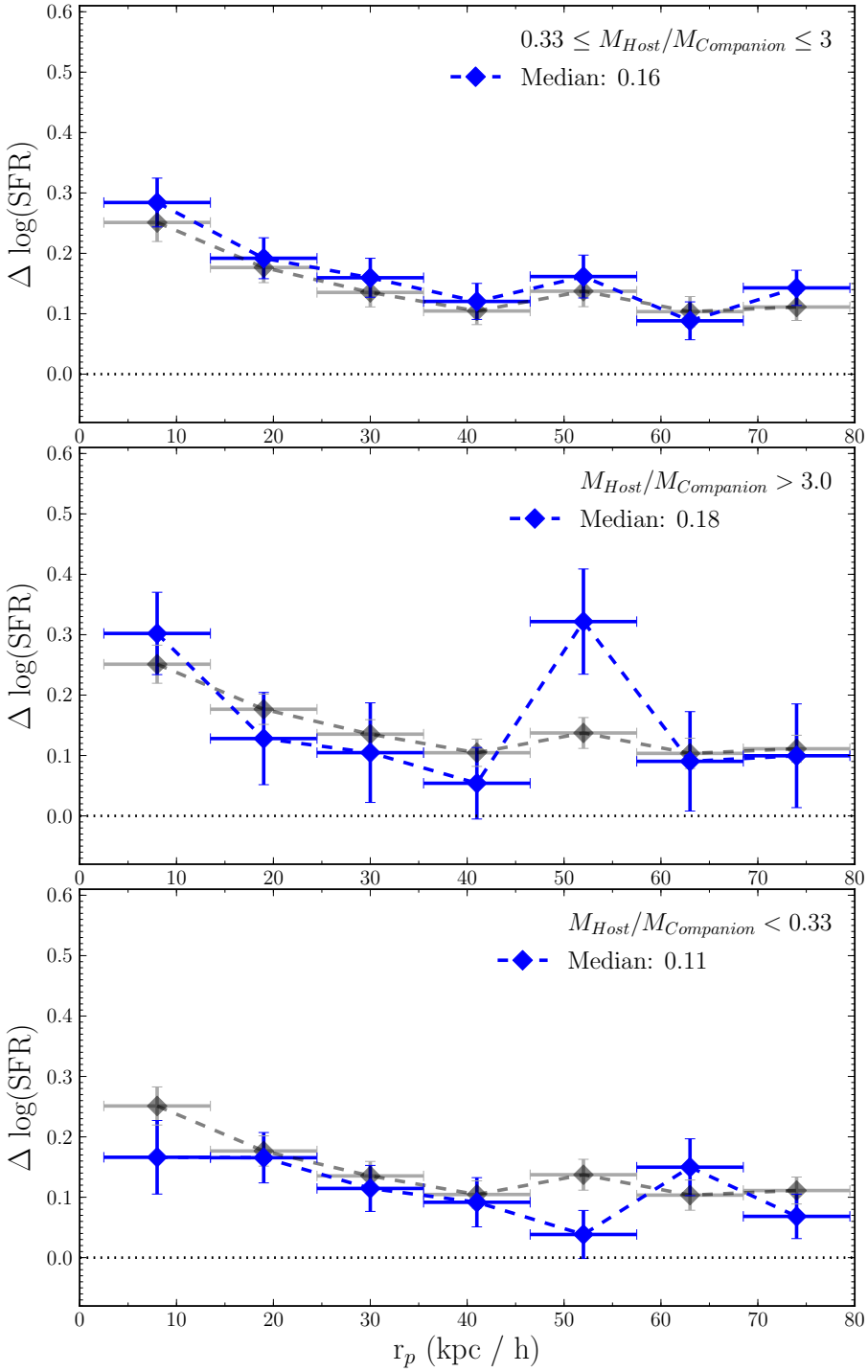

Figure 1.1: The SFR enhancement as a function of projected physical separation. The enhancement depends upon the mass ratio of the pairs galaxies, where major mergers produce consistently the largest offsets. However, significant SFR enhancement is seen in both the more and less massive companion galaxies in minor mergers. Figure from Scudder et al. (2012).

Enhanced star formation is not the only effect of mergers that we can measure observationally. As mentioned above, the increase in gas in the central region of the galaxy also has the potential to fuel an AGN. Many studies have looked at the connection between AGN and pair galaxies (e.g. Alonso et al., 2007; Woods & Geller, 2007; Ellison et al., 2008; Li et al., 2008; Ellison et al., 2011; Liu et al., 2012). Alonso et al. (2007); Woods & Geller (2007); Ellison et al. (2008, 2011) all studied the fraction of close pair galaxies that are classified as AGN compared to some defined control sample. Some studies finding an increase in the fraction of AGNs in pairs (e.g. Alonso et al., 2007; Woods & Geller, 2007; Ellison et al., 2011) and conversely no enhancement in AGN fraction (e.g. Ellison et al., 2008). Ellison et al. (2011) studied the pair AGN fraction as a function of projected separation and found that the fractional trend in the AGN is similar the trend in SFR enhancement, namely, the fraction of galaxies classified as AGN increases with decreasing separation. They also noted the same fractional trend in galaxies that are classified as composite, where composite galaxies are thought to contain contributions from both AGN and stars and suggest that their results point to enhanced AGN activity simultaneously with enhanced star formation. Other studies have also noted a connection between galaxies classified as AGN and enhanced star formation (e.g. Li et al., 2008; Liu et al., 2012; Santini et al., 2012). Santini et al. (2012), had a large sample of galaxies (not necessarily in pairs) classified as AGN and compared their star formation rates to a stellar mass and redshift matched control sample of galaxies that were not classified as AGN. They noted that in general, the galaxies classified as AGN have a larger SFR than their matched non AGN galaxies. However, their stellar mass matching is for only three bins over a large dynamic range, likewise for the redshift bins. They also do not have any information regarding the spatial information of these AGN, such as if they are in close pairs and to what extent this effects the results. Li et al. (2008) examined the Hα luminosity of pair AGN galaxies and noted that at small projected separations the AGN galaxies have an enhanced Hα luminosity over their matched control. More recently Liu et al. (2012) examined the Hδ absorption and 4000 Å break strength of interacting AGN galaxies compared to stellar mass and redshift matched isolated AGN. They noted that the Hδ absorption strength increased and the 4000 Å break strength decreased for decreasing projected separation. Both the Li et al. (2008) and Liu et al. (2012) studies conclude that, based on their respective SFR tracers, interacting AGN have enhanced star formation.

We can also measure observationally the effect that mergers have on the metallicity of interacting galaxies. Studying gas-phase metallicity, which is a measure of the galaxy's gas not locked up in stars, several studies have noted a decrease in the central or nuclear

metallicity of interacting galaxies compared to a set of control galaxies (e.g. Kewley et al., 2006; Ellison et al., 2008; Michel-Dansac et al., 2008; Scudder et al., 2012). Both the Kewley et al. (2006) and Ellison et al. (2008) studies examined the relation between luminosity and metallicity for their interacting pairs and control. Both studies found that for a given luminosity, the pairs galaxies had lower metallicities than their controls. The lower central metallicity is consistent with the inflow of metal poor gas from the outskirts of the galaxy. Scudder et al. (2012) looked at the metallicity of pairs vs. control as a function of projected separation. They found that as their projected separation decreased, so did their metallicity. Again, this is consistent with the inflow of metal poor gas to the central region.

Taking all of the observational and theoretical work together, the simplified picture of galaxy - galaxy interactions is this; galaxies come in for a passage or collision; gas loses angular momentum due to gravitational torques caused by a changing potential; gas funnels towards the central components of galaxies, which effectively lowers the metallicity in these regions; gas can reach high enough densities to fuel an intense starburst; gas can accrete onto the central black hole to fuel an AGN, where AGN galaxies can also experience an induced starburst. One of the main features of this model is that the starburst is isolated to the central regions of the galaxies. This is well supported by both theory and observations (as outlined above) for these interacting galaxies. However, do we necessarily expect that *all* induced star formation expected to occur within the central region?

1.3 Spatial properties of induced star formation

Early work by Kennicutt et al. (1987) looked at the Hα equivalent widths (EW) of interacting spirals and irregular galaxies with a close companion. They matched these interacting and irregular galaxies to a control sample of morphologically similar isolated galaxies. Kennicutt et al. (1987) noted that the spiral or irregular galaxies' Hα EWs are larger and offset from their "control" sample and that this offset is largest at small separations, which is consistent with the current model of induced star formation. Kennicutt et al. (1987) also studied the disk Hα EW and find that some disks of interacting galaxies have an enhanced Hα EW over that of their controls, suggesting induced star formation is also occurring in the disks. They note that this disk enhancement is generally present in galaxies with very large Hα EW in the nuclear region, but that the opposite is not true, large Hα in the nucleus does not mean large Hα in the disk.

Disk enhancement is supported by a few observations of individual cases of interacting galaxies as well. Some high resolution images of interacting galaxies such as the Antennae

Figure 1.2: Image of the Antennae galaxies. HII regions are noted as pink regions in the image and can be seen to dominate along the tidal features and between the two nuclei. Image Credit: NASA, ESA, and the Hubble Heritage Team (STScI/AURA)-ESA/Hubble Collaboration

galaxies exhibit regions of star formation, as inferred from HII emission, in the tidal tails or bridges between the galaxies (Figure 1.2). Klaas et al. (2010) have modelled the Antennae galaxies' star forming regions and they note that the total amount of star formation is dominated by star formation that is occurring in the arms and bridge between the two galaxies and not in the nuclei of the two galaxies. Both Jahan-Miri & Khosroshahi (2001) and Jarrett et al. (2006) have studied interacting or disturbed galaxies in a similar manner and find a similar result, i.e. that there is significant non-nuclear star formation.

In general, simulations do not yield much triggered star formation outside the central regions. Bournaud (2011) attribute the general inability for simulations to take into account or produce extended induced star formation to a lack of interstellar medium (ISM) turbulence in the simulations. However, extended star formation has been noted in some simulations already, e.g. Di Matteo et al. (2007), where they note new star formation out

to a few kiloparsecs during the interaction. Bournaud (2011) show that they are able to account for extended star formation by including ISM turbulence in their simulations. They state that the inclusion of the ISM turbulence causes non-circular motion of the gas, which can causes it to shock in the tidal features, which in turn can cause bursts of star formation.

Contrary to the evidence for disk SFR in interacting galaxies above, Ellison et al. (2010) using the bulge and disk decompositions from Simard et al. (2011) (S11), studied the bulge and disk colour distribution of close pairs compared to matched controls for different environments. Regardless of environment they found no trend in pair disk colour compared to the controls with respect to projected separation. However, in the bulge component for the low to intermediate density environments they found the bulge colours in pairs are bluer than their controls. The trend in bulge colour is similar to the trend in SFR enhancement, namely that the bulge colour is bluest at closest separations and tends towards the control value as the projected separation increases. These results suggest that, based on colours, the induced star formation is centrally concentrated and not extended to the disk.

Going beyond colours, we plan on using spectral energy distribution (SED) fitting to determine the star formation rates for a given galaxy as a whole as well as its individual morphological components, i.e. the bulge and disk components. Using the bulge and disk decompositions produced by S11, we now have an appropriately large statistical sample to help constrain spatially where induced star formation is occurring in galaxy pairs. We will be able to test directly whether the enhancement is isolated to the central regions of the galaxies as suggested by simulations and some observations or whether it is more extended, with moderate disk enhancement occurring as well. Our work will allow us to try and help disentangle the ambiguity around enhanced disk star formation.

The outline of this thesis is as follows: In chapter 2 we describe our data selection, model grid and fitting techniques. We also compare our derived star formation rates and stellar masses to other studies and outline our technique to select galaxies with constrained star formation rates. We compile our close pairs sample and outline the requirements for our control sample. In chapter 3 we derive our star formation rate enhancements for the total integrated light of the galaxy, bulge component, disk component, composite and AGN galaxies. In chapter 4 we compare our results with other current studies of enhanced star formation, and in chapter 5 we summarize our results and we conclude with a description of future work.

Throughout, we have used a cosmology of $\Omega_M = 0.3, \Omega_\Lambda = 0.7$ and $H_o = 70$ km/s/Mpc.

Chapter 2

Data and Analysis

In this chapter we describe the selection criteria used to extract the galaxies from the SDSS. We also describe the decomposition procedure performed by Simard et al. (2011) in order to derive the bulge and disk components of galaxies. We outline our model grid and our fitting algorithms and perform various tests to ensure we have the optimal setup. The spectral energy distribution production and fitting algorithms MAKE_SED and FIT_SED (Sawicki & Yee, 1998; Sawicki, 2012) are used extensively in our study, so a brief summary of what each algorithm does is given. We also outline the criteria for a galaxy to be included in our close pairs sample and the criteria for a galaxy to be included in our control pool.

2.1 Photometric data

The data we use is from the SDSS Data Release 7, Abazajian et al. (2009). Since we are using data provided by Simard et al. (2011), our selection criteria are necessarily the same as theirs but we will recap it here for completeness. Objects of morphological `type` = 3, i.e. extended objects, are selected to ensure we deal only with galaxies. A photometric cut is applied to the r-band Petrosian magnitude such that $14 \leq m_{petro,r,corr} \leq 18$, where $m_{petro,r,corr}$ is the r-band Petrosian magnitude corrected for Galactic extinction as found from the SDSS database.

For spectroscopic data, a few additional cuts are applied. Objects are required to have $m_{petro,r,corr} \leq 17.77$ and `SpecPhoto.SpecClass` = 2, i.e. the spectrum of a galaxy. Another cut on the nominal surface brightness ($\mu_{50,r} < 23$ mag arcsec^{-2}) of the galaxies is applied in order to ensure the completeness of the sample (See Figure 1 of S11) and also a redshift requirement of z > 0.005, this is to ensure the distance measurements are not contaminated

by peculiar velocities. We also take a maximum redshift of z ≤ 0.2.

S11 provide both updated photometry for galaxies in the SDSS and also derive bulge and disk decompositions for these galaxies using GIM2D (Simard, 1998; Simard et al., 2002). The updated photometry was achieved by using SExtractor (Bertin & Arnouts, 1996) for the deblending algorithm instead of the SDSS algorithm (Lupton et al., 2001) and by defining new local sky background levels. See Figure 11 of S11 and Figure 10 of Patton et al. (2011) for examples of where this new updated photometry has eliminated some problems that occur with the original SDSS photometry of close pairs.

In addition to updating the photometry for the galaxies selected from above, S11 also performed bulge and disk decompositions of these galaxies. The bulge and disk decompositions were performed simultaneously in the *g* and *r* band, while ensuring that the position angle, bulge radius, disk scale length, bulge ellipticity and disk inclination take the same values in both bands. Two other fits were performed in a similar fashion using *u* and *r* and then *i* and *r*.

The fits from GIM2D give both a total magnitude through some filter *i*, $m_{t,i}$, and a bulge-to-total flux ratio, B/T_i. The bulge and disk component apparent magnitudes, $m_{b/d,i}$, are given by:

$$m_{b,i} = m_{t,i} - 2.5log(B/T_i) \tag{2.1}$$

and

$$m_{d,i} = m_{t,i} - 2.5log(1 - B/T_i) \tag{2.2}$$

respectively, and the uncertainty for the bulge and disk component are found by

$$\sigma m_{b,i}^2 = \sigma m_{t,i}^2 + \left(\frac{2.5 \cdot \sigma(B/T)_i}{(B/T)_i \cdot ln(10)}\right)^2 \tag{2.3}$$

and

$$\sigma m_{d,i}^2 = \sigma m_{t,i}^2 + \left(\frac{2.5 \cdot \sigma(B/T)_i}{(1 - (B/T)_i) \cdot ln(10)}\right)^2 \tag{2.4}$$

where σ $m_{t,i}$ and $\sigma(B/T)_i$ are the uncertainties in the total apparent magnitude and bulge-to-total ratio in some filter *i* respectively as measured by GIM2D.

2.2 Model data

In addition to the photometric data outlined above, we need to produce synthetic model magnitudes that can be compared to the photometry and used to derive different galaxy properties. Using the Bruzual & Charlot (2003) (BC03) stellar population synthesis models, a suite of composite model spectra are constructed with varying parameters. All of the model spectra assume a Chabrier (2003) initial mass function (IMF). The model spectra all have exponentially declining star formation histories of varying strengths, characterized by their e-folding times, τ. The e-folding times lie on a semi-uniform grid to cover different physical ranges of star formation histories. Values for the e-folding time are spaced from $\log(\frac{\tau}{\mathrm{Gyr}}) = -1.5$ to -0.1 in steps of 0.2 dex and $\log(\frac{\tau}{\mathrm{Gyr}}) = 0$ to 1 in steps of 0.1 dex (Taylor et al., 2011). It is assumed that exponentially declining star formation histories will produce a more realistic picture of these galaxies' star formation than a single stellar population or constant star formation history approach.

The BC03 models initially produce a spectral energy distribution (SED) for 221 ages distributed non-uniformally from $0 - 20$ Gyr. The synthetic model SEDs are extracted from the BC03 SED model file and then interpolated on a new logarithmic grid that is distributed uniformly from $\log(\mathrm{t/yr}) = 5.1 - 10.3$ in 51 different bins. All values output from the BC03 models (e.g. SFR or mass to light ratio, M/L) are then linearly interpolated onto the new age grid. Models with ages older than the age of the universe are excluded, resulting in 50 distinct age bins.

2.2.1 Attenuation of model spectra

MAKE_SED takes a given spectrum and applies dust attenuation effects and also computes the model magnitude of the attenuated spectra through a given filter. FIT_SED takes photometric data and the model magnitudes from MAKE_SED and through χ^2 minimization derives several parameters for the source (e.g. SFR or stellar mass). See Sawicki (2012) for a complete list of supported dust laws and also for the full list of effects that can be applied to the input rest frame spectrum.

Using MAKE_SED, the newly interpolated spectra are attenuated by both interstellar dust extinction and cosmological redshift. Using MAKE_SED, interstellar reddening is applied through:

$$L_{\nu}^{'}(\lambda) = L_{\nu}(\lambda) \cdot 10^{0.4E(B-V)k(\lambda)}, \tag{2.5}$$

where $(L_\nu^{'}(\lambda)/L_\nu(\lambda))$ is the (attenuated/input) spectrum, $E(B-V)$ is the colour excess and $k(\lambda)$ is the adopted dust law, where we have chosen the Calzetti et al. (2000) dust law. The colour excess, E(B − V), ranges from 0 - 0.9 in steps of 0.05 for a total of 19 colour excess measurements. In total, accounting for the different combinations of τ, $E(B-V)$, age and Z (0.005, 0.02, 0.2, 0.4, 1, 2.5 $Z_\odot$, default BC03 values) we have 19 x 19 x 50 x 6 = 108300 models per redshift bin.

The effects of cosmological redshifting are applied through:

$$f_\nu(\lambda) = \frac{L_\nu^{'}(\lambda/(1+z))}{4\pi D_L^2/(1+z)}, \tag{2.6}$$

where $L_\nu^{'}(\lambda/(1+z))$ is the dust attenuated spectrum scaled to the desired redshift, z is the redshift, D_L is the luminosity distance and $f_\nu(\lambda)$ is the flux. The redshift bins are split from 0.01 - 0.2 in steps of 0.001 for a total of 191 different redshift bins. We use the redshift bins to fix a given galaxy's spectroscopic redshift to a particular model redshift. Fixing the redshift allows us to remove z as a free parameter and to have better constraints for our fits. Broadband SED fitting requires that we have model magnitudes as seen through some filter i. We define:

$$f_i = \frac{\int f_\nu(\lambda) FTC_i(\lambda) d\lambda}{\int FTC_i(\lambda) d\lambda}, \tag{2.7}$$

where f_i is the model flux in filter i and FTC_i is the filter transmission curve. The apparent magnitude through filter i is then found by converting f_i to an apparent AB magnitude, Oke (1974). This results in a total of 20,685,300 individual models.

2.3 Spectral energy distribution fitting - the χ^2 approach

We now investigate two methods for determining the best fit model to each set of data. Using the synthetic model magnitudes, we can now attempt to derive galaxy parameters through the use of χ^2 minimization. Here we give a description of the default χ^2 minimization technique performed by FIT_SED. The χ^2 minimization equation is defined as:

$$\chi^2 = \sum_i \left(\frac{f_{d,i} - s f_{m,i}}{\sigma_i} \right)^2, \tag{2.8}$$

where $f_{d,i}$ are data flux through filter some filter i and $f_{m,i}$ are the model flux through that same filter, σ_i is the uncertainty in the data and s is the normalization parameter and is used

to scale the model flux to the data flux. s can be found analytically by taking the partial derivative of Eqn. 2.8 with respect to s.

$$s = \sum_i \frac{f_{d,i} f_{m,i}}{\sigma_i^2} / \sum_i \frac{f_{m,i}^2}{\sigma_i^2}. \tag{2.9}$$

The quantity s is crucial in transforming the BC03 model spectra values into meaningful physical values, since the BC03 model spectra have their masses normalized to 1 $M_\odot$. FIT_SED has the ability to perform two parameter space searches to find the minimum χ^2, either brute force (full parameter space search) or a downhill[1] approach. We adopt a brute force search to derive a χ^2 value for each model input for the sake of robustness.

2.4 SED fitting - the Bayesian approach

Taylor et al. (2011) have shown that taking the minimum χ^2 is not necessarily the most desirable method (confirmed in § 2.5) since it can lead to discretized parameters (see Taylor et al., 2011, Figure 2). Instead we investigate a Bayesian approach as potentially more robust. Other studies have done a similar analysis when deriving galaxy parameters (e.g Taylor et al., 2011; Kauffmann et al., 2003; Brinchmann et al., 2004).

FIT_SED by default can only give you a single best fit model, using one of the two parameter space search techniques mentioned above. We developed a subroutine that now allows FIT_SED to derive a galaxy's best fit parameters based on the Bayesian approach. The Bayesian approach can be summarized as follows:

$$P(M|D) = P(M) \times P(D|M) \tag{2.10}$$

Where $P(M|D)$ is the probability that a given model (M) is a reliable depiction of a galaxy given the galaxy's observed SED (D). $P(D|M)$ is the probability that we will measure the observed SED assuming that the model is the true depiction of the galaxy and P(M) is the prior probability, which encodes any assumptions we make about a particular model parameter before we carry out our fits. The likelihood, $P(D|M)$, of each input model can be found from its χ^2 values through:

$$P(D|M) \propto e^{-\chi^2/2}. \tag{2.11}$$

[1]The χ^2 value of a random model is calculated and this is assumed to be the best fit model. Adjacent χ^2 values are then calculated and if one has a lower χ^2 value than the previous best fit model, this new model is adopted as the best fit model. This continues until a minimum is reached.

Bayesian statistics requires that the prior probability distribution function (PDF) be explicitly defined. Following convention (e.g. Taylor et al., 2011; Kauffmann et al., 2003; Brinchmann et al., 2004), we encode within FIT_SED a diffuse (uniform) prior PDF in age, log τ, log Z and E_{B-V}. This informs the program that we assume no prior knowledge about the distribution of our input parameters and thus do not favour any particular solutions. Therefore, the posterior PDF is essentially found directly from the likelihood values. For the sake of robustness, FIT_SED is restricted to fitting the models using the brute force method first before converting all the χ^2 values into a likelihood. This allows us to develop a full description of the posterior PDF instead of one that is broken by a downhill parameter search.

Each free parameter that goes into making up the model grid [τ, $Z_\odot$, t and $E(B-V)$] has a discrete set of initial values. The stellar mass and SFR, however, do not. Their grids must be explicitly stated, which is a direct consequence of their values being defined by the normalization parameter s and the BC03 SEDs having a normalized mass of $1M_\odot$. After defining the SFR and stellar mass grids, we marginalize over all other parameters to get the PDF of each parameter we are interested in, where the median, upper and lower sigma values are taken as the 50th, 84th and 16th percentiles respectively.

2.5 Minimum χ^2 vs. Bayesian Approach

With two possible approaches for determining the best model fit to the data, we now discuss the merits of the two techniques. As is stated above, it has been suggested by previous studies such as Taylor et al. (2011) that using the Bayesian approach to deriving galactic parameters is superior to the minimum χ^2 method. To test this statement explicitly, we select a random sample of 40,000 galaxies from our total spectroscopic sample and fit these galaxies using FIT_SED, using both the minimum χ^2 and the Bayesian methods.

Figure 2.1 shows the derived galactic parameters using the two methods. Plotted from top to bottom are τ, dust extinction and SFR all as a function of the stellar mass for both the lowest χ^2 (left column) and Bayesian most likely value (right column). Focusing on the dust extinction and τ parameters it is easily seen how the minimum χ^2 approach differs from that of the Bayesian approach. The dust extinction and τ values are limited to adopting only input grid values. As a result, these parameters are discretized with a spacing defined by the input model grid; conversely the Bayesian method eliminates the discretization of these parameters. This is due to the fact that the most likely value comes from the median of the posterior PDF of each input parameter.

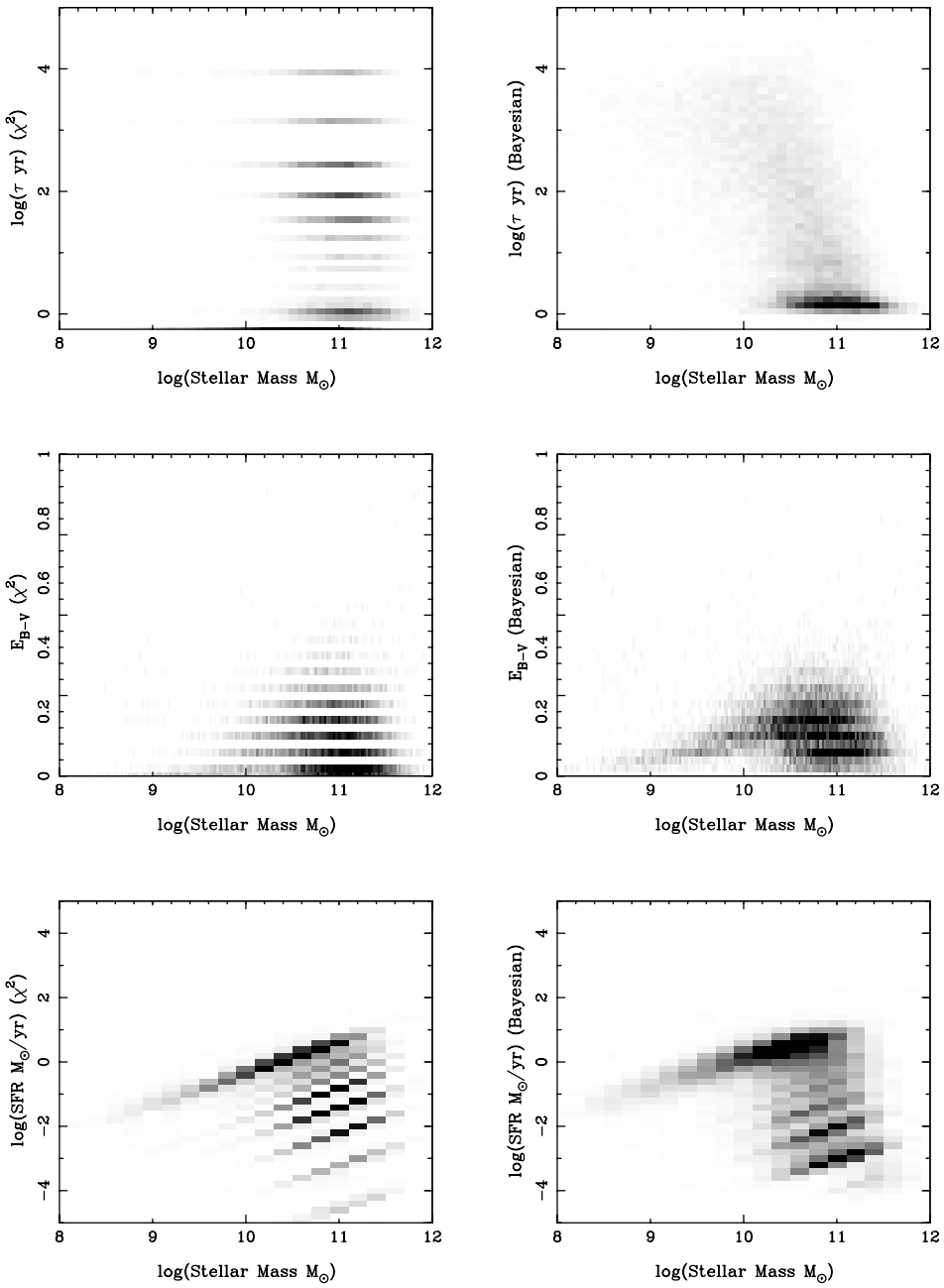

Figure 2.1: Figure to demonstrate the effects of using the most likely Bayesian approach versus that of a minimum χ^2 approach. The results for the minimum χ^2 fits are shown in the left column and those of the Bayesian approach are shown in the right hand column. The panel parameters in each column are ordered from top to bottom as the e-folding time (τ), dust extinction and SFR all as a function of the stellar mass. As can be seen in all left hand panels except that of the SFR vs stellar mass, the parameters are discretized into bins defined by the input model grid. Conversely this is not the case in the right hand panel.

The SFR vs. stellar mass panel looks similar in both cases. This is due to the fact that the parameter values are determined by the scale factor s, equation 2.9, instead of the input model grid. The two distributions, however, are not identical to one another. The reason behind this is that the most likely value comes from the median of the posterior PDF for both parameters, whereas the minimum χ^2 value comes solely from one model that was determined to have the lowest χ^2. If there are strong degeneracies between the input parameters, one can still get a non-smooth SFR or stellar mass distribution. Although we are only examining the star forming properties of these galaxies, we have elected to use the Bayesian approach over that of the minimum χ^2. The immediate advantages to using the Bayesian approach are that we avoid having discretized parameters if we were to investigate other properties of these galaxies and that the error estimate on each parameter is derived directly from its posterior PDF which uses information from the entire χ^2 distribution. The minimum χ^2 method relies on Monte Carlo iterations to derive errors, where the data are perturbed within its photometric error and the best fit is re-derived, to produce errors. These errors are still required to take values determined solely by the model grid and thus are still discretized.

2.6 Choice of grid spacing

The choice of the initial model grid spacing could potentially have an effect on the fits. To explore what effect the choice of our model grid spacing has on our fits, we examine what happens to the calculated most likely value when a grid of similar range but different spacings is used. As an example, we changed our choice of input τ values, whereby our new grid is $\log(\frac{\tau}{\mathrm{Gyr}}) = -1.5, -1.1, -0.7, -0.3, 0, 0.3, 0.5, 0.7, 1$ (compared to the old τ grid of $\log(\frac{\tau}{\mathrm{Gyr}}) = -1.5$ to -0.1 in steps of 0.2 dex and $\log(\frac{\tau}{\mathrm{Gyr}}) = 0$ to 1 in steps of 0.1 dex).

We re-fit a subsample of 40,000 galaxies with this new coarse τ grid; Figure 2.2 shows the results from this fitting. We plot a SFR − SFR plot of the coarse grid SFR vs. that of the fine grid. It can be seen that the overall shape of the SFR distribution between the fine and coarse τ grid generally follow one another. However, at very low SFRs, i.e. log(SFR $M_\odot$/yr) < -2, they diverge from one another and the fine grid returns SFR values that are greater than the coarse grid's SFRs. To further illustrate the agreement between the two fits, we plot in Figure 2.3 a histogram of the differences of the two absolute values of SFR (from both the fine and coarse grid). Figure 2.3 shows that $\approx 60\%$ of the galaxies have SFRs that agree with one another within ± 0.05 dex.

Since the absolute value of the SFR is interpolated as the median value of the posterior

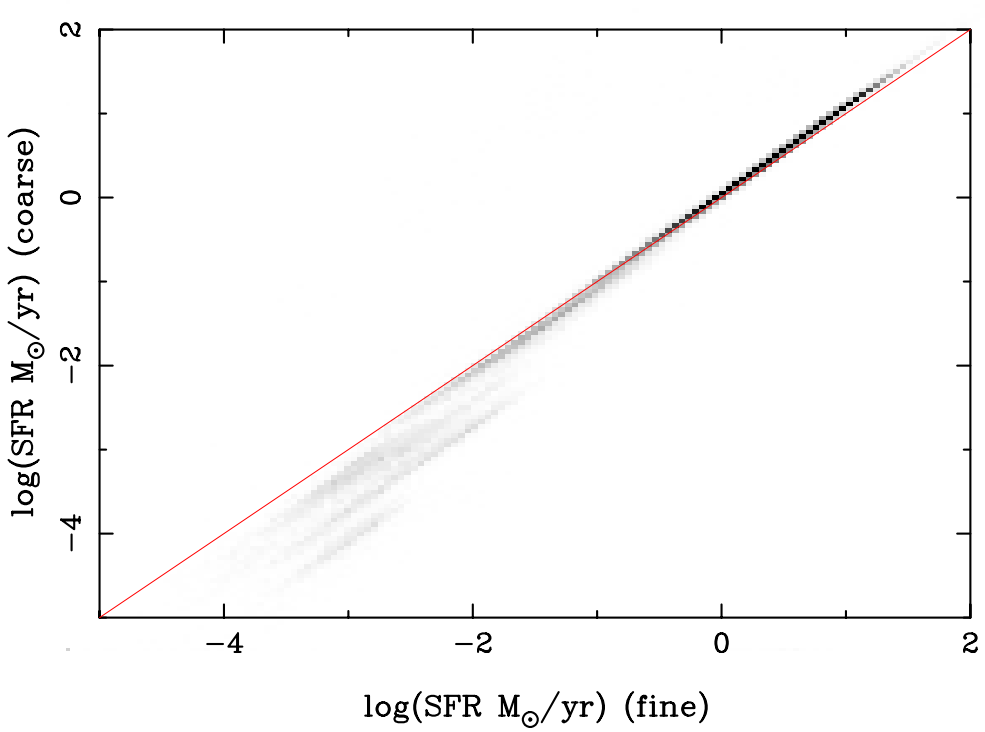

Figure 2.2: A SFR − SFR plot comparing the fine and coarse τ grid absolute values of SFR. The red line shows the 1:1 agreement we would expect if the two values of SFR agreed perfectly with one another. There is overall excellent agreement between the samples. The values do diverge from the 1:1 line at low values of SFR, where the fine grid produce larger SFRs.

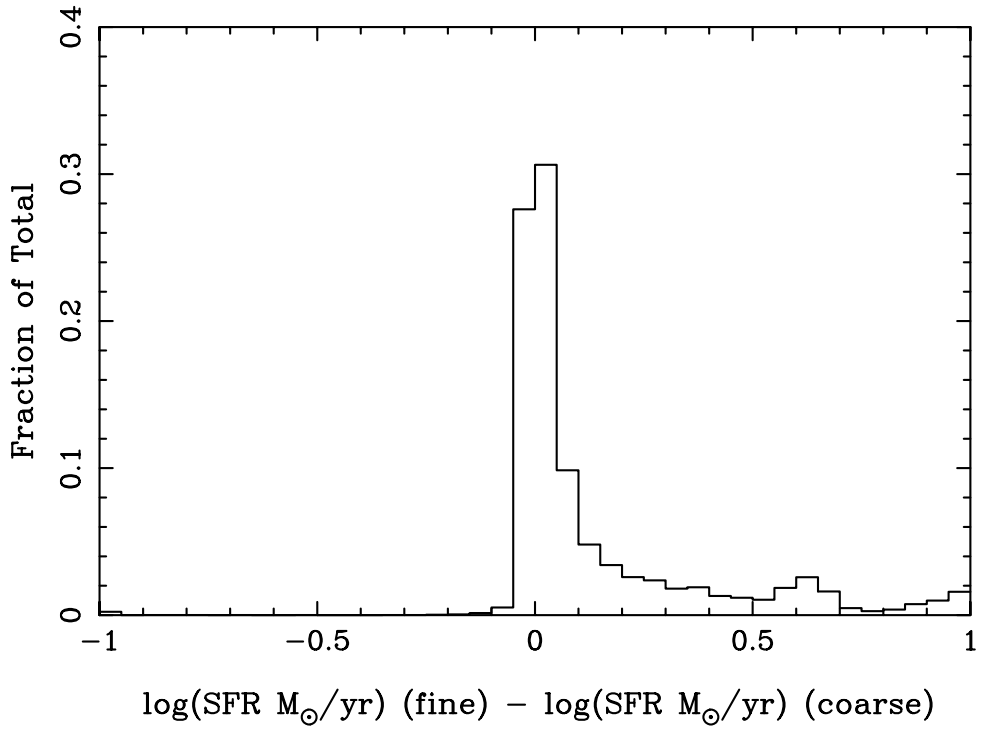

Figure 2.3: The distributions of the differences between the SFR from the fine and coarse grid. This plot showcases what was seen in Figure 2.2 in that generally the SFRs agree within ± 0.05 dex.

SFR PDF, as long as the τ parameter is adequately sampled in an appropriate range, the finer spacing in between seems to have little effect on the overall SFR distribution to a degree. As we will show later, at very low SFRs our fits become poorly constrained, so that the fine and coarse grids agree over the range that we will utilize SFRs. Even though the absolute value of the SFR seems to not have a strong dependence on the spacing of the τ grid, we continue to use the fine spaced τ grid since it is more evenly sampled.

2.7 Choice of softening parameter

Generally, when broadband SED fitting is performed, one adds a softening in quadrature to the photometric error of each band. The softening is an important parameter, as it prevents some models from having an infinite χ^2 value by forcing a floor on to the σ_i values (see Equation 2.8). The softening is not a measure of the reliability of the photometric error, however, it is a constant value that is added in quadrature to the photometric error and is also designed to take into account any uncertainties that may be present in the synthetic models used when comparing to photometry. The true value of the softening parameter that should be used is hard to quantify and we explore what happens when we vary this parameter. We select a random subsample of 40,000 galaxies from the full spectroscopic sample and perform SED fits to these galaxies using different softening values. We selected values of the softening of 0.001, 0.03, 0.05, 0.08 and 0.1 magnitudes.

Since we are primarily interested in the star formation properties of galaxies we focus on this particular parameter. We are not concerned with the absolute values of the SFR as of yet, because we will ultimately study the relative difference in SFRs between sets of galaxies (pairs and controls). For this reason, we split our random sample in two and look at the relative difference between SFRs of each galaxy in our first half and their corresponding galaxies in our second half. We do this for each softening value. The results of this analysis are presented in Figure 2.4 which shows the cumulative fraction of galaxies as a function of their SFR difference. Figure 2.4 shows that when looking at the difference between SFRs, the slope of the distribution increases as you increase the softening. Table 2.1 shows the median value of the differences in SFRs plus the upper and lower 1 σ value.

As can be inferred from Figure 2.4 and seen directly in Table 2.1 the median difference in SFR for all values of softening are consistent with one another within their 1σ errors. However, the difference between the upper and lower 1 σ values consistently decreases. This is interpreted to be due to the fact that when an artificially large error is introduced, the photometric data now has the opportunity to explore more models that otherwise would

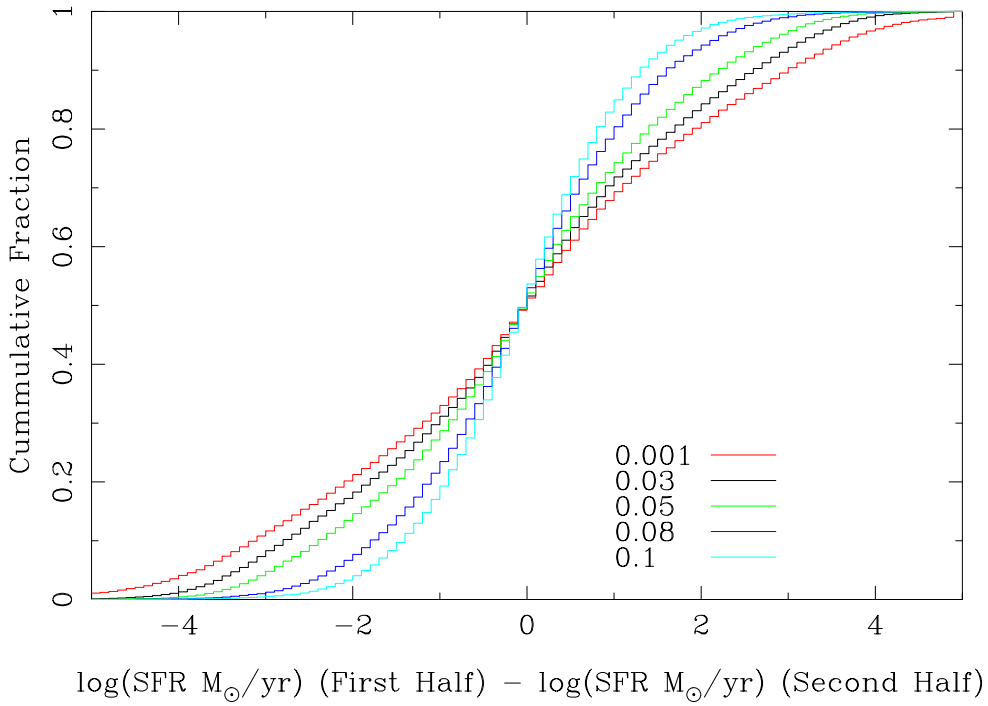

Figure 2.4: Cumulative distributions of SFR differences for a given softening. The median values of the distribution agree within the errors (Table 2.1). However, it is noted that the distribution becomes tighter as we increase the softening.

Medians of SFR differences			
Softenings	Median	Lower 1σ	Upper 1σ
0.001	−0.011	−2.469	2.332
3 0.03	−0.021	−2.175	2.026
0.05	−0.028	−1.829	1.704
0.08	−0.039	−1.334	1.236
0.1	−0.041	−1.096	1.004

Table 2.1: Median values of SFR differences from Figure 2.4 and their 1 sigma errors.

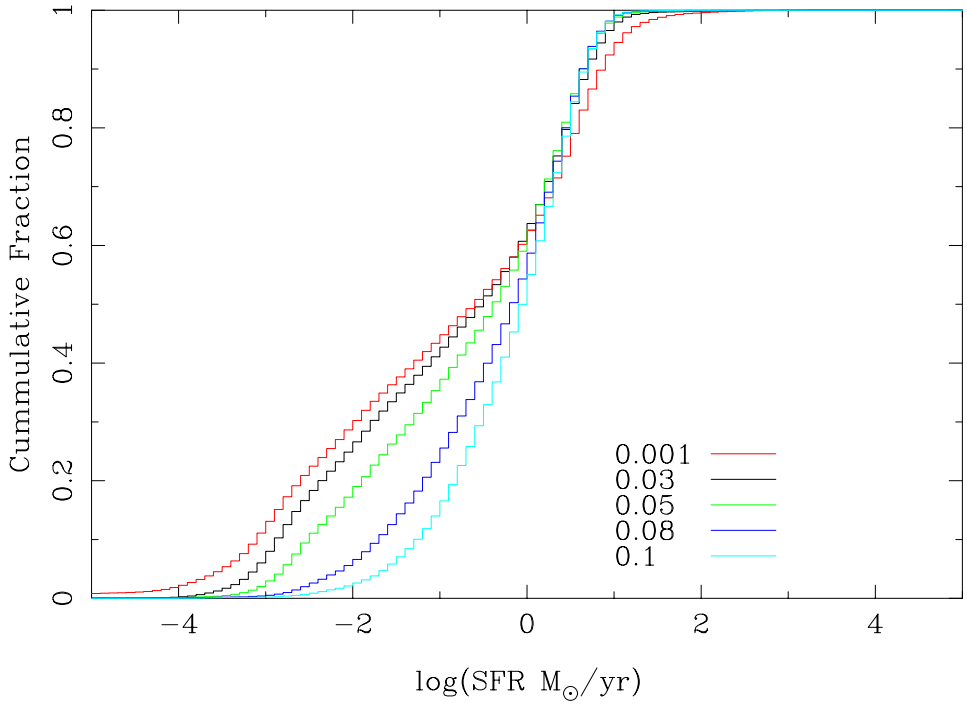

Figure 2.5: Cumulative distribution of the absolute values of SFR for a given softening. The low end of the SFR distribution is shifted towards higher values as the softening is increased. This causes the increase in the slope seen in Figure 2.4.

have given a large χ^2 value, i.e. very low probability. This causes the absolute SFRs of the galaxies to adopt values that are more homogenous with one another, which is shown in Figure 2.5, where we have plotted the cumulative distribution of the absolute values of SFR. Figure 2.5 shows that as you increase the softening parameter you shift the previously low SFR galaxies towards higher SFRs. The same analysis is done for the specific star formation rate (sSFR), Figure **??**, where it can be seen that there is excellent agreement between softenings of 0.03 magnitudes and higher for a sSFR value of log(sSFR /yr) > -10.5.

One should be cautious and understand that the absolute value of the SFR has a dependence on the value one adopts for the softening parameter. However, the absolute determination of this value is difficult to quantify. Due to the fact that we ultimately study the relative SFRs (pairs versus controls) which seems to have little effect on the median rela-

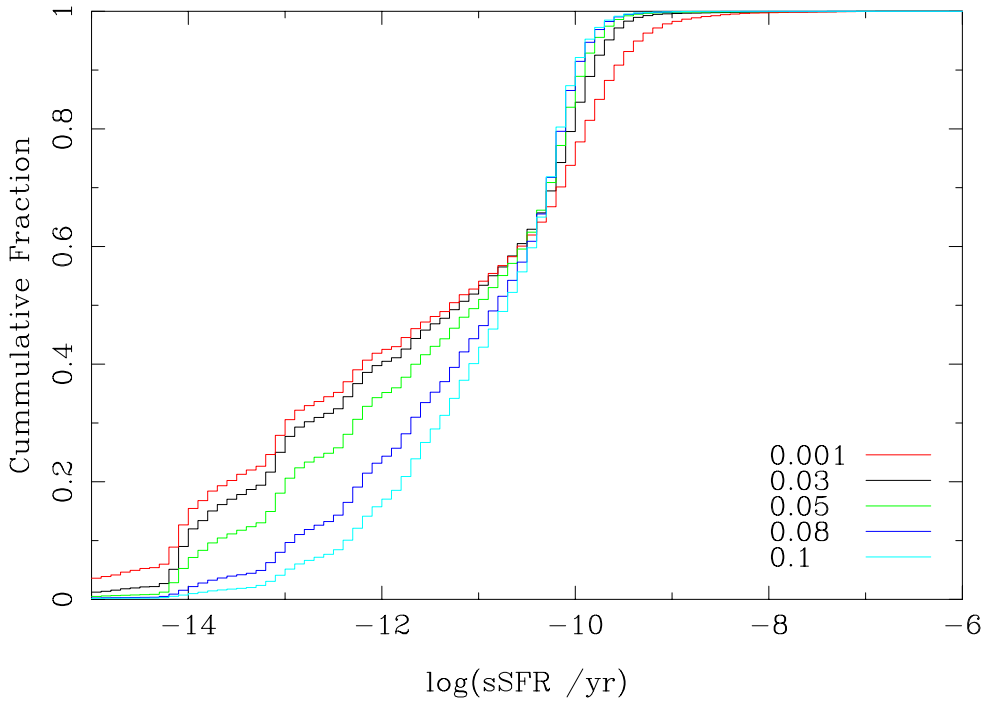

Figure 2.6: Cumulative distribution of the specific star formation rates for a given softening. As in Figure 2.5, it is seen that the low specific star formation galaxies are systematically shifted to higher values for larger softening magnitudes. Above a value of log(sSFR /yr) > -10.5 there is generally good agreement between the distributions regardless of the softening magnitude.

tive difference (Figure 2.4) we have selected a softening value of 0.03 magnitudes, which is similar to the value adopted by other studies, such as Taylor et al. (2011) who use 0.05 magnitudes. This selection is motivated by Figure 2.5 where it can be seen that above log(SFR $M_{\odot}$/yr) > 0 there is excellent agreement on the absolute values of SFR for softenings of 0.03 magnitudes and higher.

2.8 Comparison of SED fitted values with previous studies - SFRs and stellar masses

After performing the above tests we can now SED fit the total, bulge and disk magnitudes of each galaxy as derived from GIM2D with assurance that we have a robust model grid and fitting technique. To see how our fits compare to previous studies we compare the SFR and stellar mass from the model SED fits to those derived using the emission line/calibration techniques of Brinchmann et al. (2004) (B04) for SFRs and photometric fits of Kauffmann et al. (2003) for total stellar mass in order to check whether or not we reproduce comparable results with our 4 band SED fitting. First we look at the comparison between our SFRs and those of B04 updated based on the work of Salim et al. (2007) and aperture corrected to a global SFR.

The B04 SFRs were calculated using both emission lines and calibrations (see below) based on a subset of their galaxies. The technique can be summarized as follows:

• Absorption lines were modelled using BC03 burst models and subtracted from the SDSS spectra.
• Emission lines were modelled using Charlot & Longhetti (2001) models.
• A suite of models was constructed and using a Bayesian approach, PDFs were made for parameters they were interested in (e.g. dust attenuated SFR and dust attenuation)

The B04 SFR method above pertains to galaxies classified as star forming (see below) since it is primarily based on emission line diagnostics. For other classifications of galaxies, i.e. AGN or no Hα, SFRs are calculated using a relation between the specific star formation rate (sSFR) and the 4000Å break. This calibration was set up using the sSFR-4000Å relation defined by the galaxies that were classified as star forming. For each galaxy, a new sSFR-4000Å relation is constructed using galaxies of similar dust attenuation as defined by the ratio between Hα/Hβ. These SFRs are for fibre values only and B04 had to apply aper-

ture corrections in order to estimate the total SFR of the galaxy which is what we compare our fits to. B04 apply aperture corrections by first finding the light outside of the fibre and then fitting this light to stochastic models. The total SFR is then the SFR from the fibre added to the SFR from the stochastic[2] models .

B04's classifications of galaxies was carried out by using the position of each galaxy on a Baldwin et al. (1981) (BPT) diagram which focuses on a galaxy's emission line properties. B04 use a combination of four emission lines, [O III]λ5007, Hβ, [N II]λ6584 and Hα and using the ratio of log([O III]λ5007 / Hβ) vs. log([N II]λ6584 / Hα), a cut can be made to determine what the main ionization source for the galaxy is, i.e. stars or AGN. Much work has been done to help distinguish between the different populations on the BPT diagram. Using both stellar population synthesis and photoionization models Kewley et al. (2001) (K01) placed an upper limit on the regime where galaxies that are considered to be star forming are located. Above the K01 line the emission line strengths cannot be explained by stars alone and therefore an additional ionizing source, i.e. AGN, are expected to dominate. Using a more empirical approach, Kauffmann et al. (2003) K03 revised the demarcation downwards between star forming and AGN, where galaxies that lie in between these two demarcations are now considered to be composite galaxies, where it is thought that they can have contributions from both stars and AGN. These demarcations can be seen in B04's Figure 1. Stasińska et al. (2006) have their own demarcation between star forming and AGN classification, that is similar to the K01 diagnostic but uses updated models, we do not include this demarcation because it was not available to B04 and we are comparing directly against them. For a galaxy to be classified as star forming, B04 require that each emission line has signal-to-noise (S/N) > 3 and lie below the K03 line. Composite galaxies are galaxies that have a S/N > 3 in all four lines and that are classified as star forming by K01 but AGN by K03. AGN are required to have S/N > 3 in all four lines and lie above the K01 demarcation. Low S/N star forming galaxies are whatever galaxies are left after the above component have been removed and that have a S/N in Hα > 2. "No Hα" galaxies consist of galaxies that had weak or no emission lines and could not be classified on a BPT diagram.

Figure 2.7 shows the SFR − SFR plot of all galaxies in the DR7 spectroscopic sample, with a 1:1 line shown in solid black. There are two prominent populations of galaxies. There is an group of galaxies parallel to the 1:1 line, where the SED SFR values return a greater SFR for a given galaxy then B04, typically by ≈ +0.1 dex. There is also a large tail

[2]Models that are not defined by a fixed grid of input parameter values. They are defined by a random distribution of input parameter values between an upper and lower limit for each respective parameter.

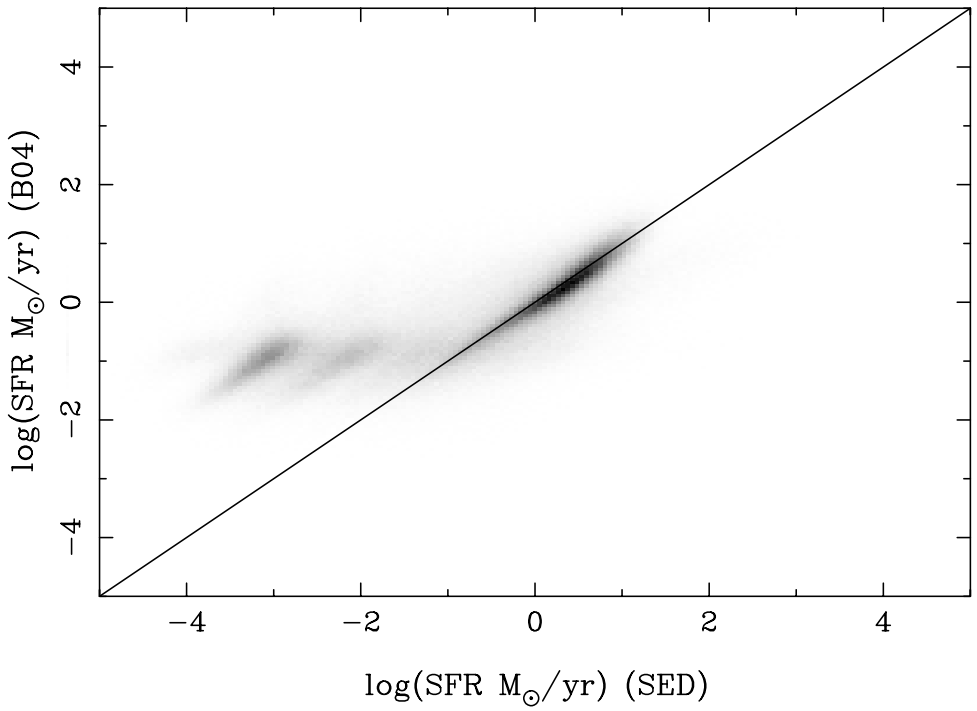

Figure 2.7: The comparison between the star formation rates derived from the emission line/calibration diagnostics of Brinchmann et al. (2004) and those found from SED fitting. Two prominent distributions are seen, one following but slightly offset from the 1:1 line and tail at the low star formation regime of both methods.

of galaxies at the low SFR end of both the B04 SFR and the SED SFR where the B04 SFRs are higher than our own. Following the example of Salim et al. (2007), we investigate what part of the SFR − SFR plot different classifications populate, i.e. whether a given galaxy is classified by B04 as AGN or star forming.

Figure 2.8 shows the SFR − SFR plot for the different classifications of galaxies. It can be seen that galaxies classified as low S/N star forming, composite and AGN all generally populate the parallel 1:1 region on the SFR − SFR plot and as discussed in § 2.10, the statistics of these galaxies should be dominated by well constrained SFRs.

The galaxies classified as star forming by B04 are shown in the lower panel of Figure 2.8. These galaxies again occupy the 1:1 area from Figure 2.7, however, their distribution is much tighter than the other classifications.

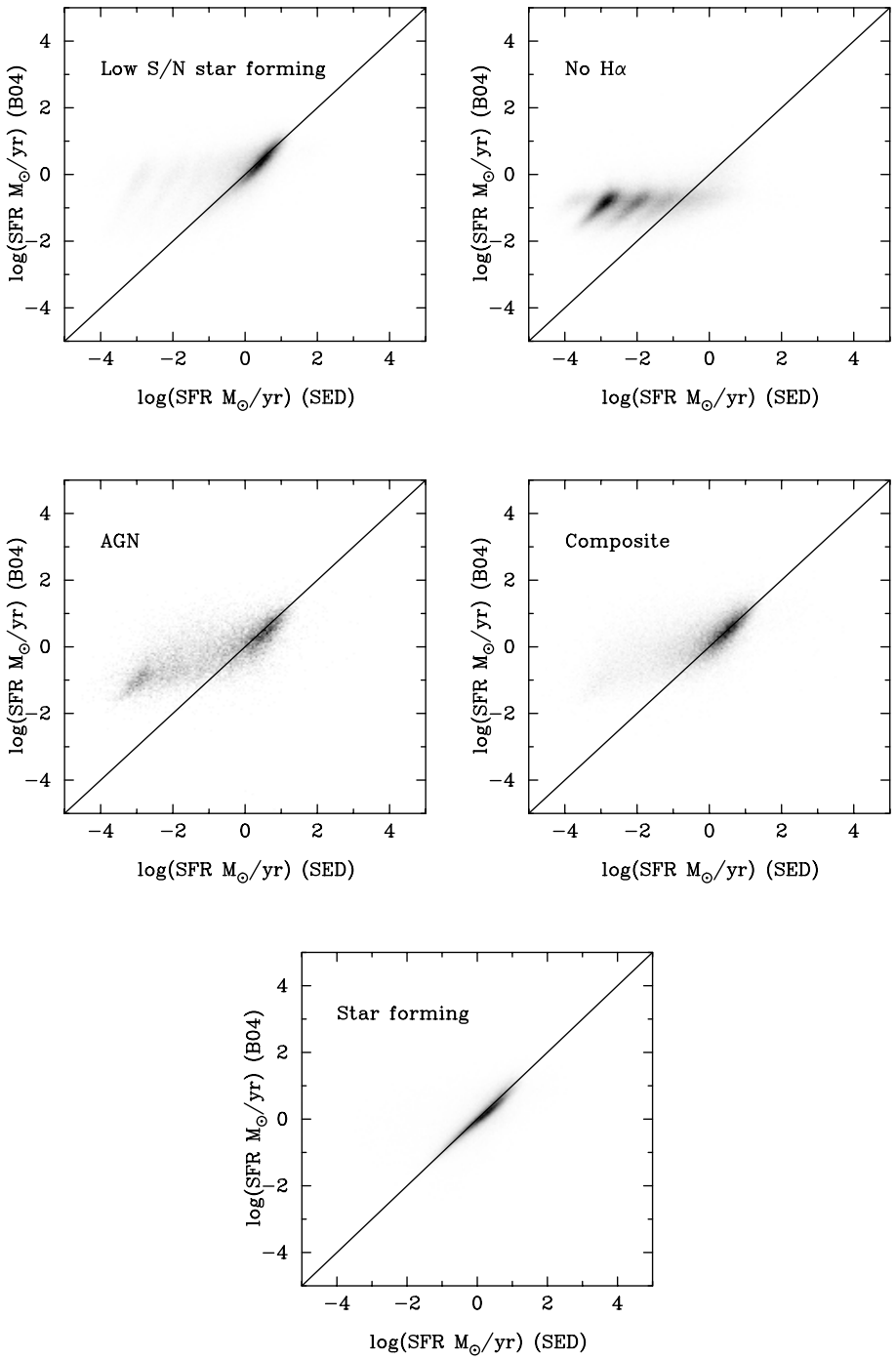

Figure 2.8: Different galaxy classifications defined by Brinchmann et al. (2004) and where on the SFR - SFR plot these are located. It can be seen that although the SED fitting produces SFRs with a much larger dynamic range, most classifications have galaxies that are slightly offset from the 1:1 line. The galaxies that are classified as having no Hα and to a lesser extent, some AGN are shown to dominate the low SFR tail in both methods where SFRs are poorly constrained.

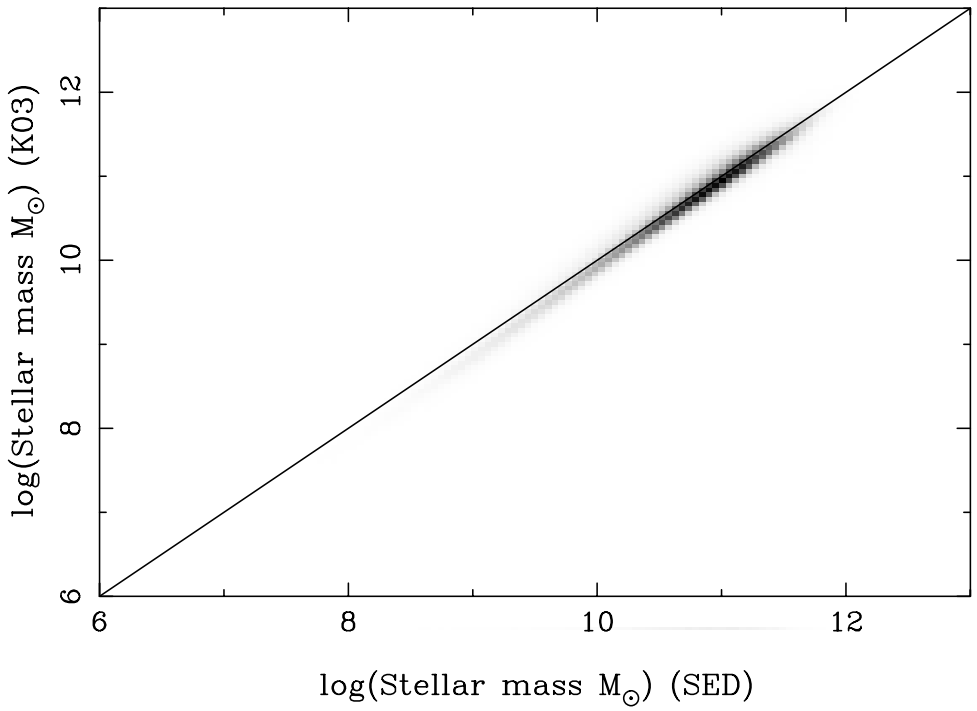

Figure 2.9: The comparison between the stellar masses derived from the photometry fitting of Kauffmann et al. (2003) and those found from SED fitting. There is overall good agreement between the two methods, with the SED stellar masses being offset by ≈ 0.1 dex.

The galaxies classified as having no Hα detection can be seen to dominate the low SFR locus that is present in Figure 2.7. This is not surprising since these galaxies generally consist of red sequence galaxies, which in our case have poorly constrained SFRs.

We now examine how our stellar masses compare to the stellar masses derived by Kauffmann et al. (2003). We follow a similar analysis as we performed for the SFRs. We first examine the total stellar mass distribution between the two studies. Figure 2.9 shows the total stellar mass − stellar mass plot for the full spectroscopic sample. As can be seen there is very good agreement between the stellar masses in the two studies although, the stellar masses found from our study appear to be ≈ 0.1 dex higher than the stellar masses of Kauffmann et al. (2003).

Again, it is worth while to break our analysis down to the individual classification of

galaxies to see if one particular type of galaxy is dominating the small offset we see. Figure 2.10 shows the same analysis as Figure 2.8, this time presenting the stellar masses instead of SFRs. Figure 2.10 shows that all classifications of galaxies are generally offset from the Kauffmann et al. (2003) masses by ≈ 0.1 dex with some classifications having slightly more width to their offset than others, i.e. AGN compared to star forming. There are some underlying differences in our model grids and in order to try and pin down our offsets these differences warrant investigation.

2.9 Differences in model grids

Although we produce comparable SFRs and stellar masses, there are three major differences between our models and those of B04 and Kauffmann et al. (2003):

1. We use magnitudes from GIM2D, whereas the MPA group use SDSS model magnitudes. GIM2D total magnitudes are slightly brighter than SDSS model magnitudes (see Simard et al., 2011, Figure 8).

2. The model grid used by B04 and Kauffmann et al. (2003) has bursts of constant star formation superimposed on their initial exponentially declining star formation history.

3. We use a Calzetti et al. (2000) dust extinction law, where B04 and Kauffmann et al. (2003) use a Charlot & Fall (2000) dust law.

We test the first issue directly by refitting a sample of 40,000 galaxies using our initial model grid, where we now use the SDSS model magnitudes instead of those provided by GIM2D, S11. We look at the SFR $-$ SFR relation for our SFRs derived using both sets of data, where we only plot galaxies that have been classified as star forming by B04. Figure 2.11 shows that there is generally good agreement between the SFRs calculated using both the GIM2D and SDSS magnitudes. Figure 2.12 shows the relation between the stellar mass estimates using these different magnitudes. Again there is excellent agreement between the two estimates.

We next test whether or not the inclusion of bursts of star formation in the model grid has a systematic effect on the derived SFR. To test this we look at the Hδ absorption line strength for each galaxy. As outlined in Kauffmann et al. (2003) the equivalent width (EW) of the Hδ line is a good diagnostic to test whether there has been a recent burst of star

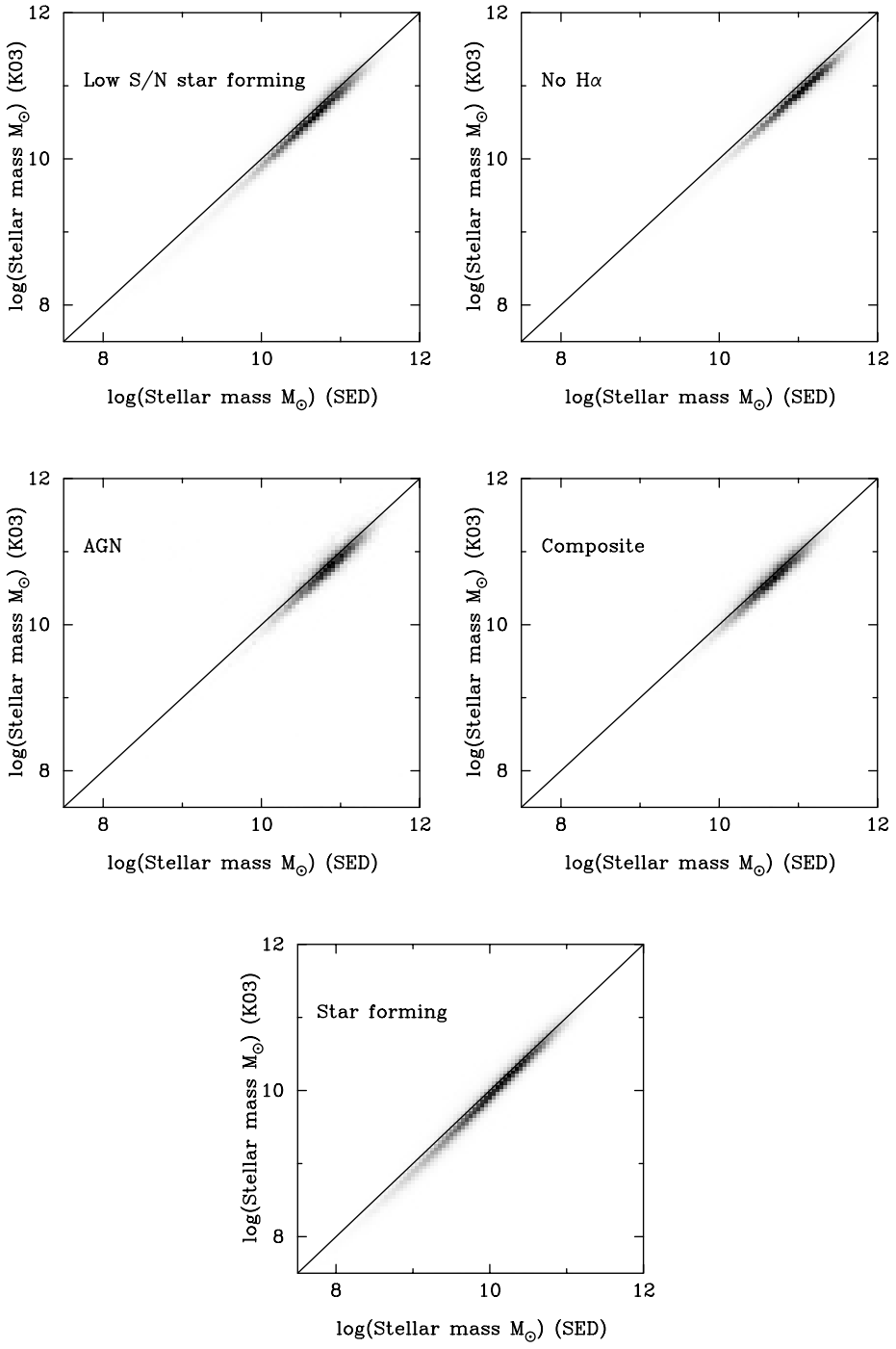

Figure 2.10: Different galaxy classifications defined by Brinchmann et al. (2004) and where on the stellar mass - stellar mass plot these are located. Regardless of classification the masses seem to be robust and all classifications give comparable results.

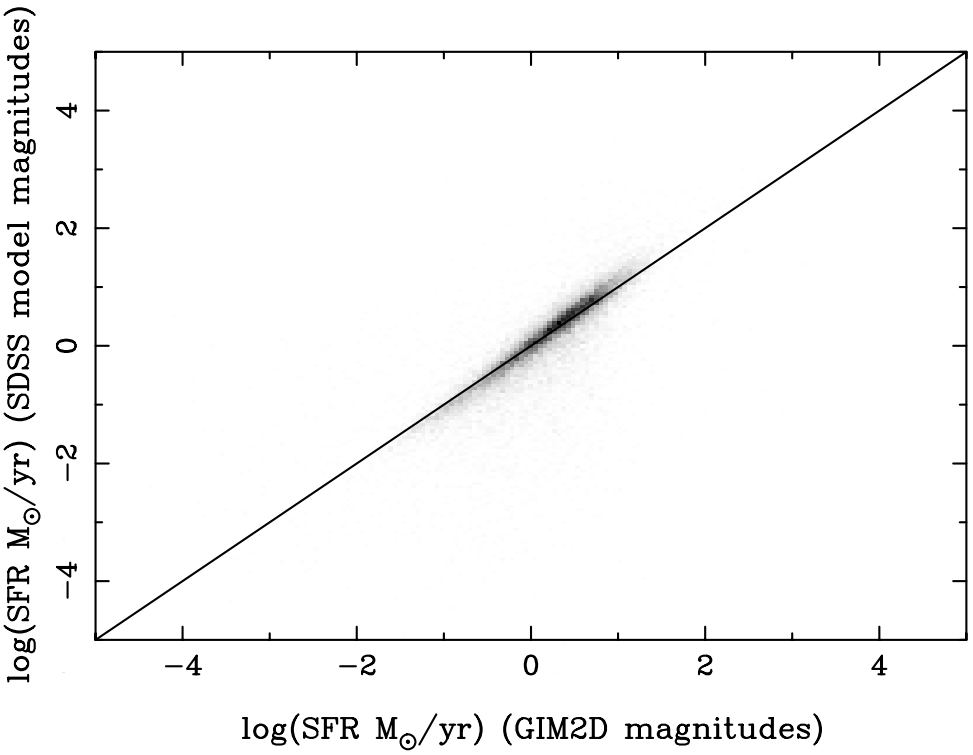

Figure 2.11: The comparison between the star formation rates derived from the GIM2D magnitudes and from SDSS model magnitudes for galaxies that are classified as star forming. There is no offset observed when we switch from GIM2D to SDSS model magnitudes.

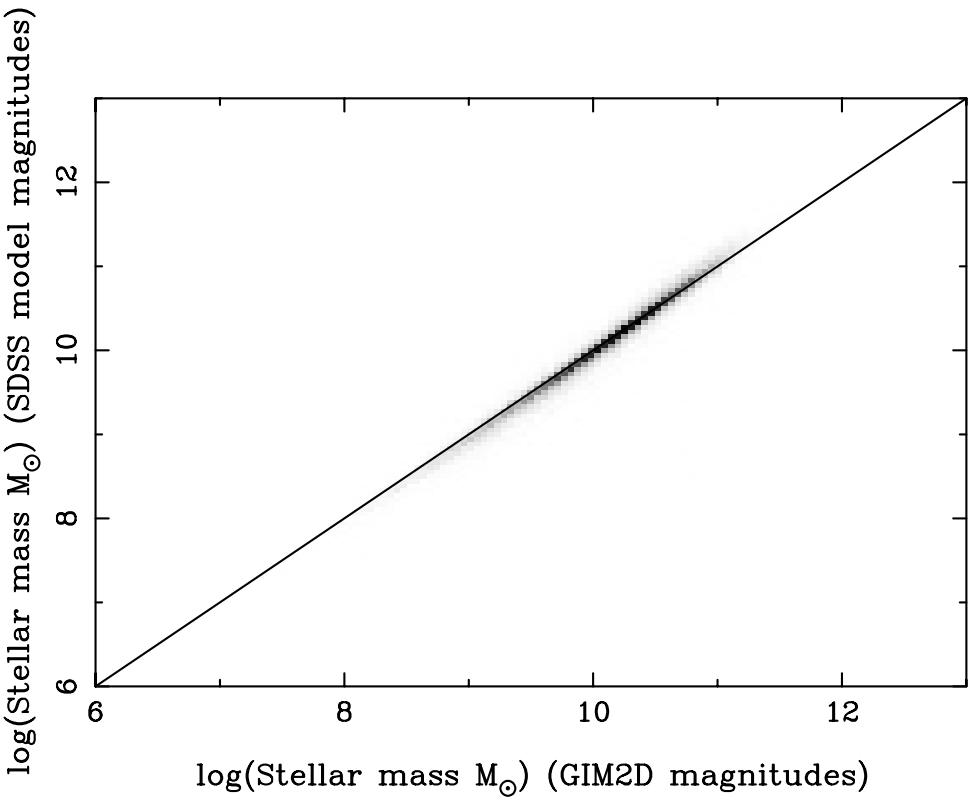

Figure 2.12: The same as Figure 2.11 except we now plot stellar masses.

formation. We look at three different situations. The first is galaxies which have a Hδ EW ≥ 6Å, which have a high probability of having undergone a burst within the last 2 gigayears and galaxies with $2 \leq$ Hδ EW ≤ 3Å, which is a combination of bursting and non-bursting models of varying strengths and lastly, galaxies with Hδ EW ≤ -1 Å which are galaxies that should not have undergone a recent burst of star formation.

Figure 2.13 shows the results of this analysis. The cases with positive Hδ strength are both generally offset from the 1:1 line by the same amount, ≈ 0.1 dex, with the high EW Hδ galaxies forming a tighter relation around the 1:1 line. The H$\delta \leq -1$ Å sample has relatively few galaxies in it since we are using galaxies that are classified as star forming by B04. However, for the few galaxies it does contain there is a larger concentration around the 1:1 line. It appears the addition of bursts of constant star formation on the underlying exponentially declining star formation history model does not lead to large discrepancies when comparing the absolute values of our SFRs to those of B04. The same trend is observed in the stellar masses of the galaxies, Figure 2.14.

We also test what effect changing from the Calzetti et al. (2000) dust law to the two component Charlot & Fall (2000) dust law used by B04 has on the derived SFRs of the galaxies. We construct a new model grid with all parameters identical to our initial grid, with the exception of the dust law parameters. The Charlot & Fall (2000) dust law is parameterized by two different variables, τ_v, which is the total effective V-band optical depth and μ, which is the fraction of the total effective V-band optical depth contributed from the interstellar medium. We adopt τ_v values of 0.1, 0.5, 1, 1.5, 2, 2.5, 3.5, 5 and 6 and a constant $\mu = 0.3$ (default BC03 value). This is a slightly different grid than that used by B04 and Salim et al. (2007), who adopt a random distribution of τ_v centred at 2 and μ centred at 0.3. Figure 2.15 shows the SFR $-$ SFR plot between our new SFRs using the Charlot & Fall (2000) dust law and that of B04. As can be seen the galaxies are offset parallel from the 1:1 line, with smaller SED SFRs than B04 even when fitting with a very similar model grid by ≈ 0.1 dex. The stellar masses we report using the Charlot & Fall (2000) dust law are larger than before, with an offset ≈ 0.2 dex from 1:1. This description of the Charlot & Fall (2000) dust law is not complete in the sense that we do not take a stochastic approach to our fits and our priors are flat distributions, however these simple tests gives us confidence that out results are relatively robust against changes to the model grid and input data.

It is worthwhile to appreciate that if we are looking for a SFR enhancement as a function of pair separation relative to a control sample, the absolute value of our SFRs do not necessarily have to agree on a one to one basis between different studies. A parallel offset

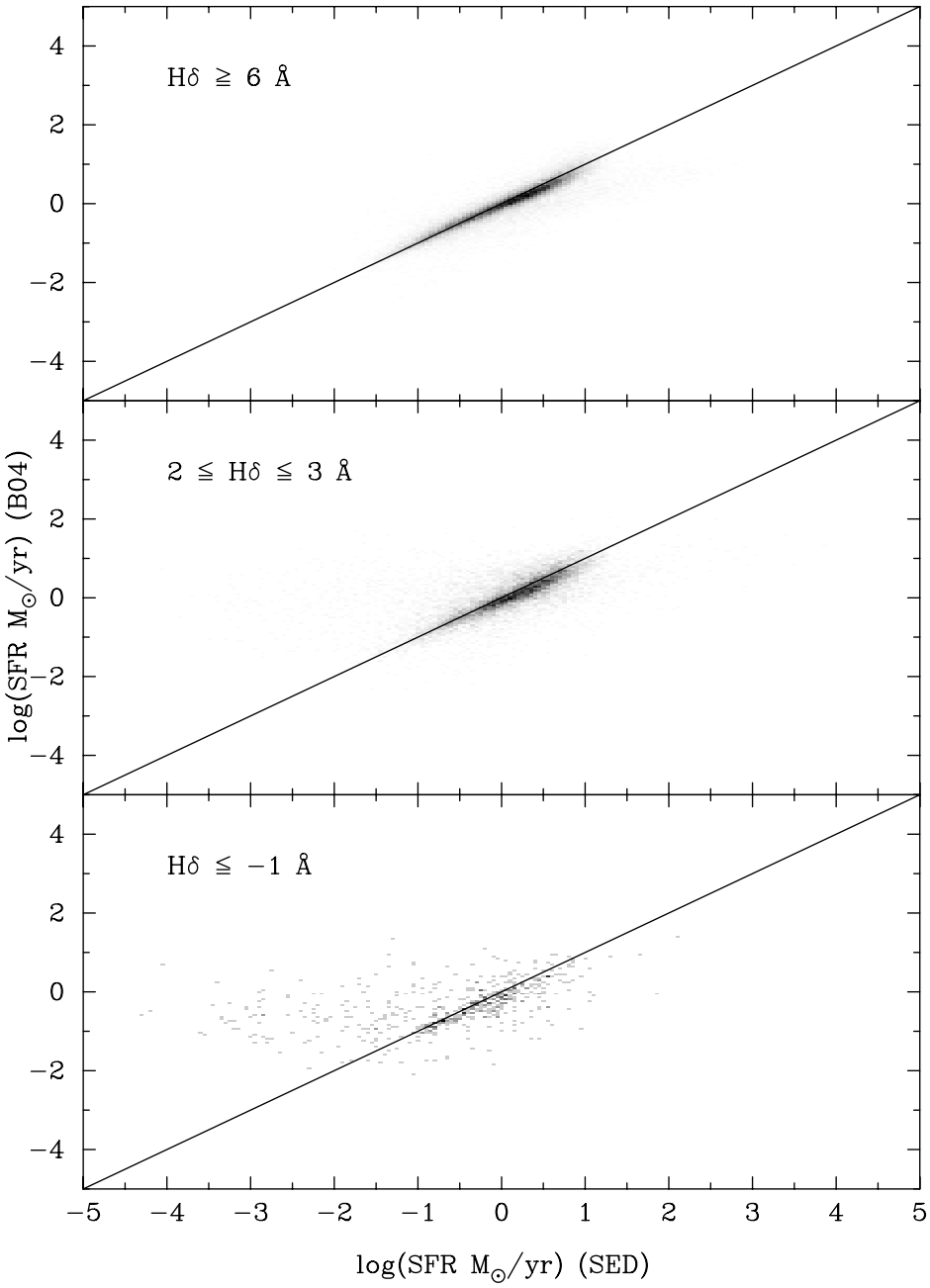

Figure 2.13: The comparison between the star formation rates derived from the emission line/calibration diagnostics of Brinchmann et al. (2004) and those found from SED fitting for galaxies of varying Hδ strength classified as star forming. There is no discernible difference between the high Hδ and intermediate Hδ case which indicates that the inclusion of bursts in the model does not affect strongly the derived SFR. The low Hδ case has a wide spread of SFR values, with a concentration centred around the 1:1 line.

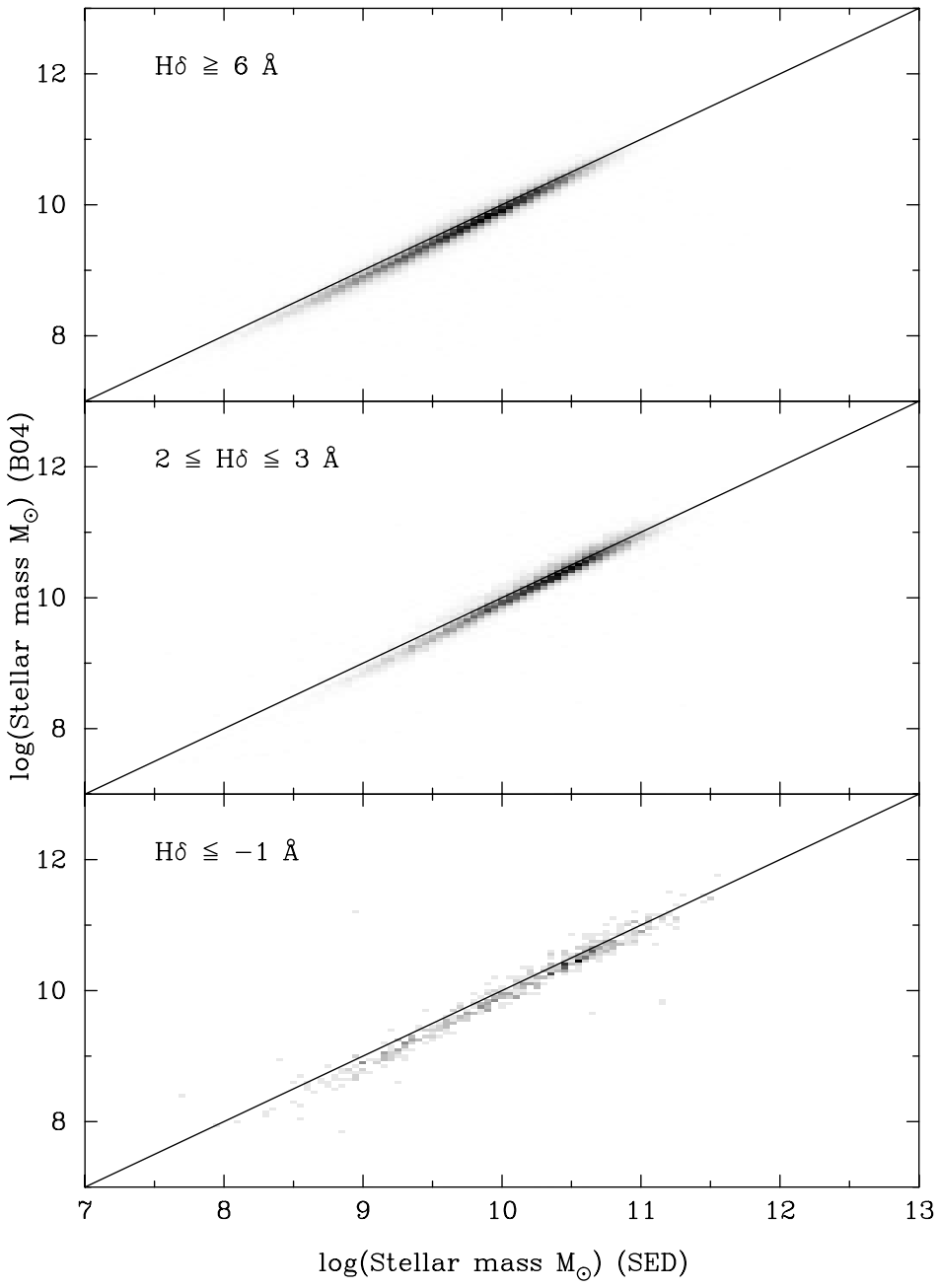

Figure 2.14: Same as Figure 2.13 except with stellar mass now plotted. The addition of bursts does not seem to effect the determined stellar mass

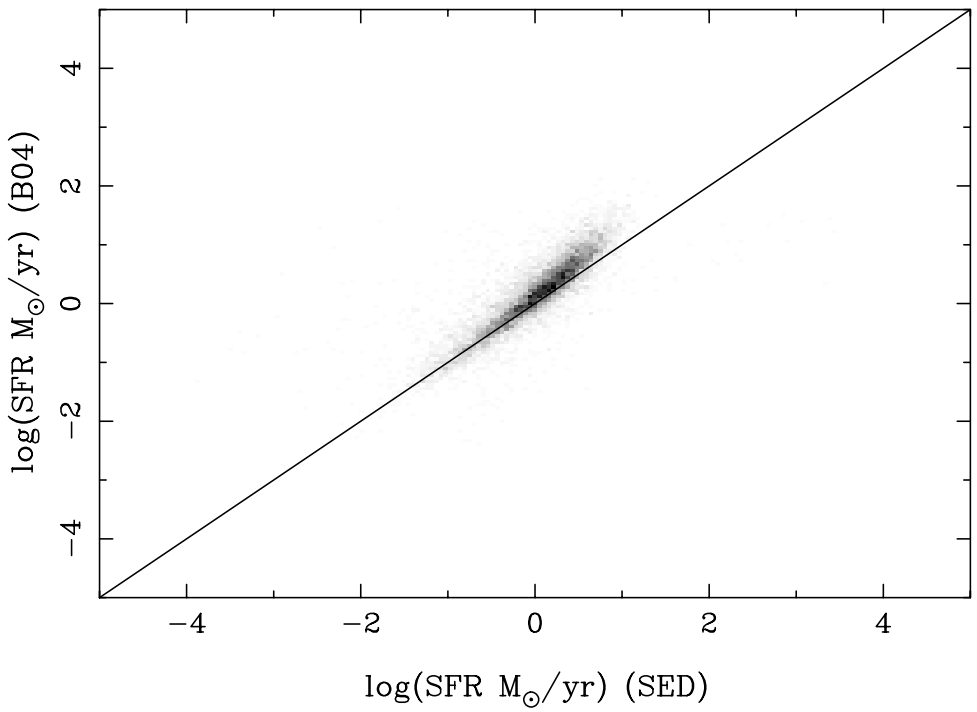

Figure 2.15: The comparison between the star formation rates derived from the emission line/calibration diagnostics of Brinchmann et al. (2004) and those found from SED fitting using the Charlot & Fall (2000) two component dust law for galaxies classified as star forming. The difference between the SED and B04 values is ≈ 0.1 dex.

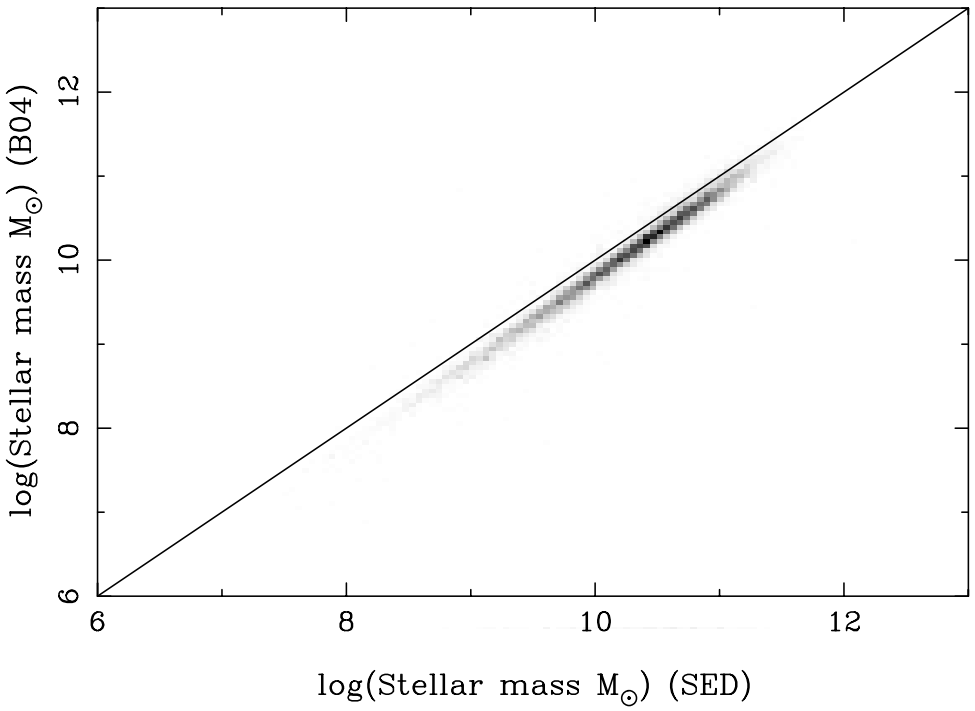

Figure 2.16: Comparison of stellar masses where we now include the Charlot & Fall (2000) dust law. The SED fit masses are shifted towards larger values and are now offset by ≈ 0.2 dex.

will not affect the results as long as we are looking at the relative difference between SFRs of galaxies. From the above, it can be concluded that although we do not have an exact 1:1 relation between B04 and our SFR values, the SFRs in general agree well with one another. Therefore we conclude that our derived 4-band SFRs are sufficient for our purposes.

2.10 Extracting reliable SFRs from photometric SED fitting.

In general any method used to determine the properties of galaxies, such as SFRs, will break down at one point or another. We therefore want to understand where this breakdown occurs between our values and B04. We do this by studying the distribution of specific star formation rates, sSFRs, of the two studies. We compare sSFRs due to both our stellar masses and SFRs being offset from B04 by ≈ 0.1 dex each. The offset in stellar mass and SFR equates to consistent measures of sSFR.

Figure 2.17 shows a histogram of sSFRs. Our SED sSFRs are shown as the solid black line, and the B04 values are shown as a black dashed line. It can immediately be seen that there is excellent agreement at the high sSFR end, $\log(\text{sSFR /yr}) \gtrsim -11$, between the two distributions. The distribution of galaxies in this regime is dominated by galaxies that were classified as star forming by B04. Below a value of $\log(\text{sSFR /yr}) \lesssim -11$ our values no longer match the B04 values and tail off towards extremely low values. We want to only consider galaxies where both B04's sSFRs and our sSFRs agree well with one another. Therefore, we fit a Gaussian function to our high sSFR peak, shown as the blue histogram in Figure 2.17 and the point where the contribution from well constrained galaxies falls below 90% is shown by the red vertical line in Figure 2.17. This occurs at a sSFR value of $\log(\text{sSFR /yr}) = -10.45$. We assume that below this value, we no longer have the ability to reliably report on a galaxy's SFR.

It is worth while to understand which galaxies we primarily include by imposing a sSFR cut to the sample. To investigate this, we plot where the galaxies that pass our sSFR cut lie on a colour magnitude diagram (CMD). The top panel of Figure 2.18 shows the $(u - r)$ vs M_u CMD for all galaxies that we fit. One can note on this figure both the red sequence and the blue cloud, where the red sequence is generally considered to be red elliptical galaxies and the blue cloud can be thought of as blue spiral galaxies. The bottom panel of Figure 2.18 shows the galaxies that were selected based on our sSFR cut overlaid on top of the original CMD, as red dots. It can be seen that the galaxies that are generally selected to

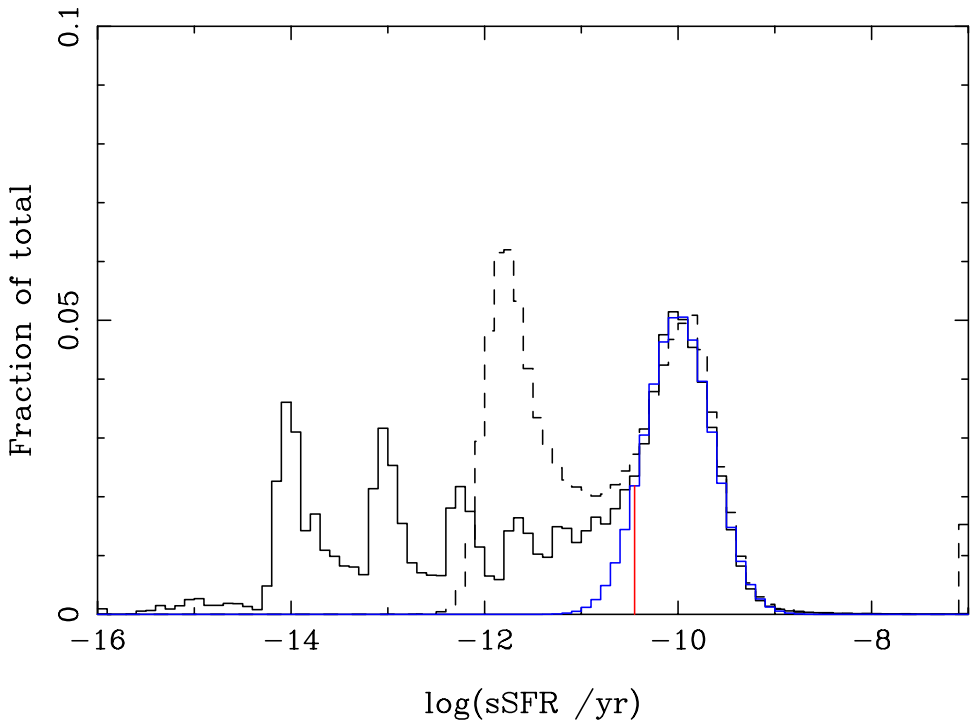

Figure 2.17: The specific star formation rate distribution of all galaxies in our spectroscopic sample plotted as the solid black histogram. The dashed histogram shows the sSFRs of B04. There is good agreement between the high sSFR end of the distributions, both in shape and magnitude. A Gaussian is fit to the high sSFR end (blue line) and the red vertical line signifies our sSFR cut to extract galaxies with reliable SFRs.

have well constrained sSFRs are galaxies that reside in the blue cloud. This is an expected result since it is generally these galaxies that are considered to be star forming and thus we should be able to constrain their SFRs. [3]

2.11 Pair Sample

Having calculated stellar masses and SFRs for the full spectroscopic SDSS catalog using S11's updated photometry, and having imposed cuts to ensure a reliable sample, we now define our sample of close pairs. For a given galaxy, a close pair is defined as two galaxies that satisfy several different criteria:

1. A projected physical separation of $r_p \leq 80$ kpc/h.
2. A line of sight rest frame velocity difference of $\Delta v \leq 300$ km/s.
3. A stellar mass ratio between the given galaxy and its companion of $0.1 \leq M_1/M_2 \leq 10$.

Our pair selection criteria are also limited to one companion per galaxy, thus if more than one close companion is found, the galaxy with the smallest r_p is taken as the companion. Patton & Atfield (2008) quantified the incompleteness of close pairs in the SDSS due to fibre collisions and using this Ellison et al. (2008) estimated that 67.5% of interacting galaxies with an angular separation < 55" are absent from the SDSS spectroscopic sample. Thus, following the example of Ellison et al. (2008), 67.5% of pairs with an angular separation > 55" are excluded in order to account for this incompleteness at small separations. This ensures we have a uniform sample that is not biased towards higher angular separations. We also require that the galaxies pass our sSFR cut (although its companion need not).

After all the above criteria are applied to the data, a total of 4,797 galaxies with a close companion are found.

[3] Another option instead of a post facto sSFR cut is a colour cut on the photometry before it is fit. This could be justified from Figure 2.18 where it is shown that that we deal mostly with blue cloud galaxies when looking for constrained SFRs. However, we did not want to make a colour cut on our sample because colour folds in several parameters such as age, SFR and metallicity.

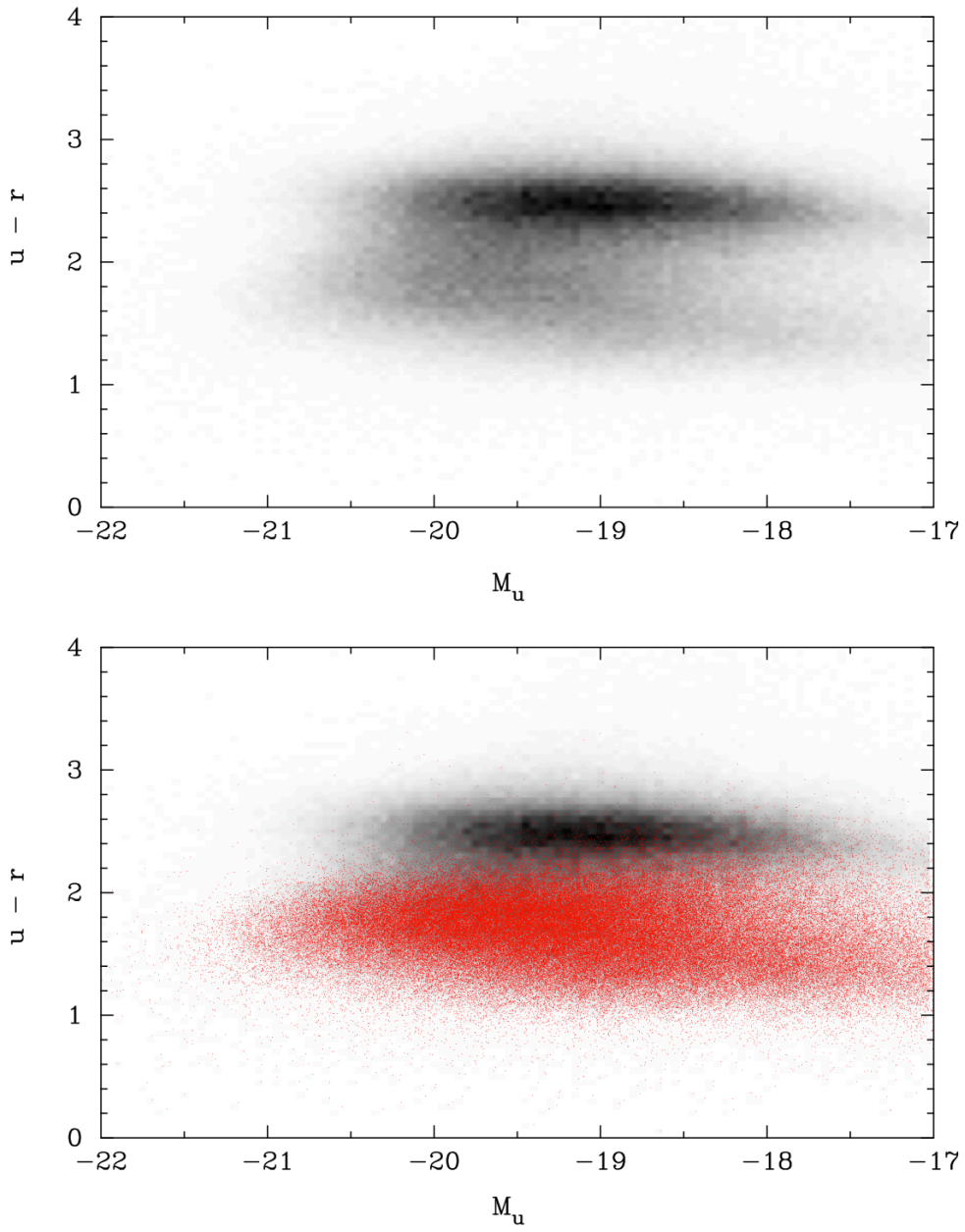

Figure 2.18: Colour magnitude diagram for all galaxies in our spectroscopic sample in the top panel. The red sequence and blue cloud are clearly seen in this distribution. The bottom panel has the galaxies that pass our sSFR cut overlaid as red points; these occupy mainly the blue cloud portion of the CMD.

2.12 Control Sample

A robust control sample is needed in order to assess the effects of interactions and mergers on paired galaxies (Perez et al., 2009). The control sample is compiled from the remaining spectroscopic galaxies that were not classified as close pairs.

In order to assign a control galaxy to a pair galaxy, a simultaneous match in redshift, stellar mass and local density/environment, calculated using the 5th nearest neighbour density, normalized to the median density, within a redshift window ± 0.01 around the galaxy, is performed. For each pair galaxy, a unique control galaxy is found that is best matched simultaneously in the three parameters and also passes the sSFR cut. A Kolmogorov-Smirnov (KS) test is performed between the pair galaxies and matched control galaxies distributions in redshift, stellar mass and environment to ensure they are not drawn from different populations. If the KS test returns a result > 32% (1σ) for each criterion, the potential controls are accepted as part of our control sample. The matching process is repeated without replacement until the KS probability drops below 32% (1σ) in any one of the parameters (z, stellar mass or environment).

Each control galaxy is then assigned its paired galaxy's projected physical separation from its neighbour (r_p), stellar mass ratio and Δv in order to be able to determine what kind of dependence these parameters play in galaxy mergers. A total of 10 unique controls per pair galaxy are matched before the KS test fails, a total of 47,970 controls. Figure 2.19 shows the distributions of both the pair and its matched control sample in both redshift, stellar mass and environment. From this point onwards all results are derived using galaxies that pass the sSFR cut unless otherwise stated. It can be seen that the two distributions (pairs and control [red line]) agree well with one another (Figure 2.19). We will additionally be studying the spatially resolved SFRs of bulges and disks, but defer those sample definitions until § 3.3.

2.13 Summary

In brief, the major components of this chapter are:

1. We constructed a model grid using the BC03 synthetic spectra models. We attenuated these spectra to include the effects of dust and cosmological redshifting.

2. We developed a Bayesian technique to be used with FIT_SED that is shown to produce results that are non-discretized, which is commonly the case with a maximum

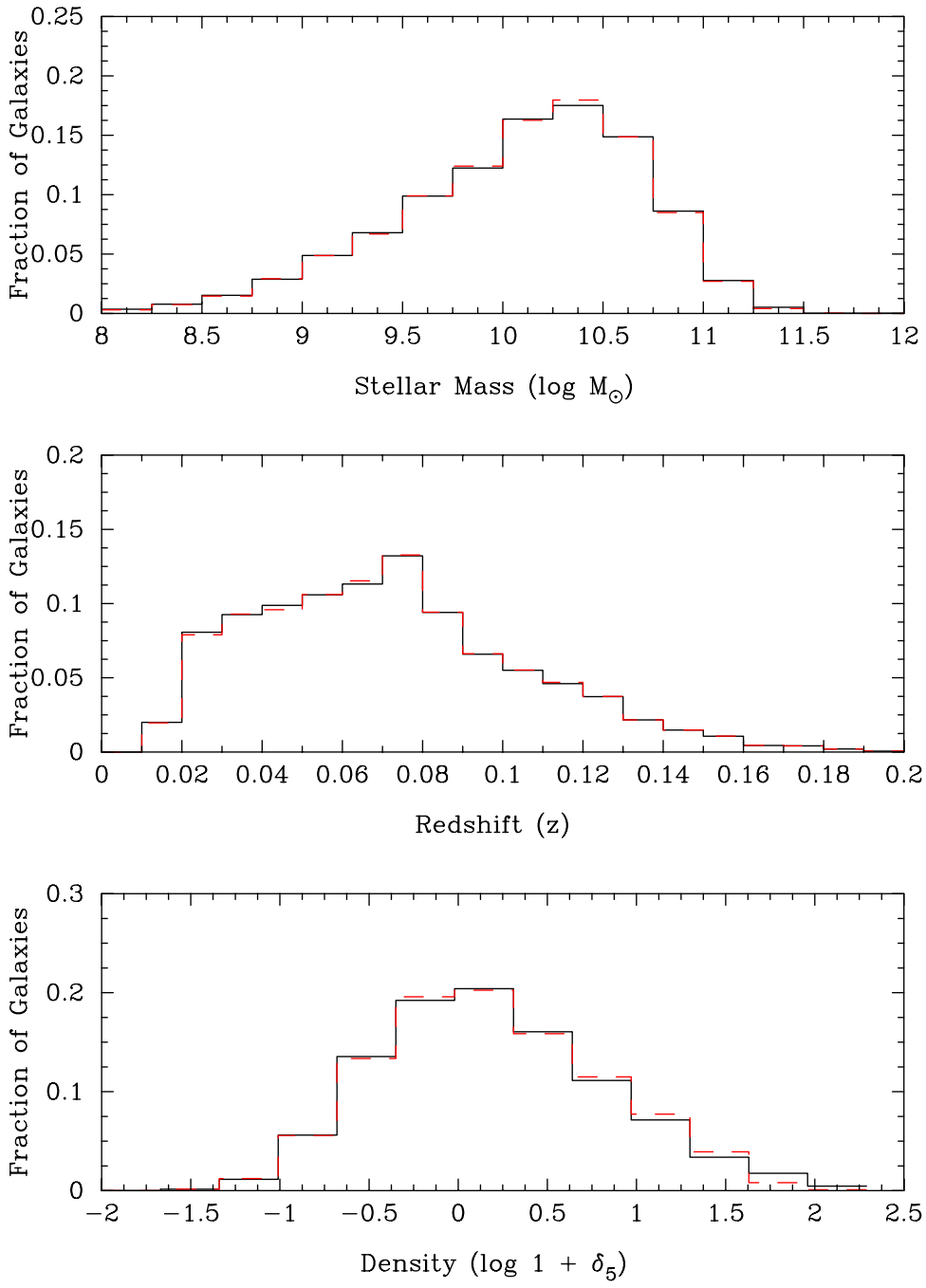

Figure 2.19: The distributions of both the pair (solid black) and control (red dashed) galaxies with respect to the matching parameters (z, stellar mass and environment) for galaxies that pass the sSFR cut. A total of 10 galaxies per pair were matched before the KS test fails for a total of 47,970 control galaxies.

likelihood approach.

3. We compared our SFRs and stellar masses against B04 and Kauffmann et al. (2003) and found we reproduce stellar masses that wholesale offset by ≈ 0.1 dex higher than Kauffmann et al. (2003) regardless of galaxy classification and SFRs that are one average ≈ 0.1 dex higher for galaxies not classified as having "No Hα".

4. We developed a sSFR cut that allows us to extract galaxies that are generally considered to be star forming and that have well constrained SFRs. This cut becomes necessary when looking at different morphological components where spectroscopic classifications may not be attainable.

5. We constructed a close galaxy pairs sample as well as a robust control sample that is matched in stellar mass, local density/environment and redshift.

Chapter 3

Results

In this chapter we investigate the effect that merging has on the star formation rates of close interacting galaxy pairs. We first examine the star formation rates for the total integrated light to understand what happens to the galaxy in a general sense. We then break our analysis down into separate galactic components, i.e. the bulge and disk component of the galaxies, to examine the spatial dependence of merger induced triggered star formation.

3.1 Pairs Offset

Using the galaxy pair and control samples defined in § 2.11 and 2.12 we can now examine what effect galaxy interactions play on the star formation rates of these galaxies. Since our fitting method gives us the entire SFR PDF for each galaxy, we would like to use all the information contained in that instead of the absolute value of SFRs taken from the median of that SFR PDF. By taking the median we could be losing information unnecessarily from the two ends of the distribution that may be important. We therefore use the normalized SFR PDFs of each galaxy to calculate a relative SFR enhancement between pair and control galaxies. We break the pair and control sample up into different projected physical separation, r_p, bins from $0 - 80$ kpc/h in bins of 10 kpc/h. For each r_p bin we take all the SFR PDFs of the pair galaxies that lie in that bin and stack them to get what we term as a "super"-PDF; the same is done to the control galaxies. This gives us a SFR PDF describing the SFR properties of all pairs present in a particular r_p bin and also the control SFR properties. An example of what these distributions look like is shown in Figure 3.1, where we present the (pair/control) super-PDFs as the (black/red) line for the inner most r_p bin. Figure 3.1 shows that these two distributions do not lie on top of one another, suggesting

that they have different star formation rates. The relative enhancement between the pair and control galaxies is then calculated by taking the cross correlation of the pair super-PDF against the control super-PDF in each r_p bin. The results of this cross correlation are shown in Figure 3.2 as the filled circles, where the errors come from $\sigma / \sqrt{N_{pairs} + N_{control}}$ [4].

Figure 3.2 shows that the relative SFR enhancement between close pairs and their controls is largest at small separations, reaching a peak enhancement of ≈ 0.25 dex which corresponds to about a factor of 2 increase of SFR in interacting pairs. We also note that for a significant range of projected separations, i.e. $20 \leq r_p \leq 60$ kpc/h, that our SFR enhancements are flat and show no increase or decrease, forming a kind of "plateau" (e.g. Patton et al., 2011; Scudder et al., 2012). The SFR enhancements in this plateau are at a magnitude of ≈ 0.15 dex. We also note a small increasing enhancement out at the larger separations.

3.2 SFR enhancement - all galaxies

The sSFR cut predominately selects galaxies that are star forming. The previous SFR enhancement (Figure 3.2) was exclusive to these sSFR selected galaxies. However, we can address the question of SFR enhancement in a more general sense by considering all galaxies in our pairs sample before the sSFR cut is applied.

Since galaxies with unconstrained SFRs generally have flat SFR PDFs, it may be assumed that when we stack this PDF with that of a galaxy that is highly star forming, the unconstrained galaxy's PDF will simply act as a floor, contributing equal probability at all points and will not change the overall shape of our super-PDF. If this is the case we can potentially still derive a measurable enhancement from the galaxies that are contributing an appreciable amount of star formation when we exclude our sSFR cut and use all galaxies.

We reconstruct a pairs sample from §2.11 where we do not require the pairs to pass the sSFR cut and we then match a control sample to these pairs. We have 13,954 pairs with 27,908 control galaxies that were not required to pass the sSFR cut (i.e. 2 control per pair). Figure 3.3 is the same as Figure 3.2, except this time the full pairs sample with no sSFR cut is used and their appropriately matched controls. Immediately, one can see that the signature of the star formation rate enhancement that was formerly detected when the sSFR cut was applied is dramatically decreased. This new analysis is likely telling us about the combination of the offset for the pairs from their controls and on the relative

[4] σ is estimated as the range in Δ log(SFR) between the 16^{th} and 50^{th} percentile values.

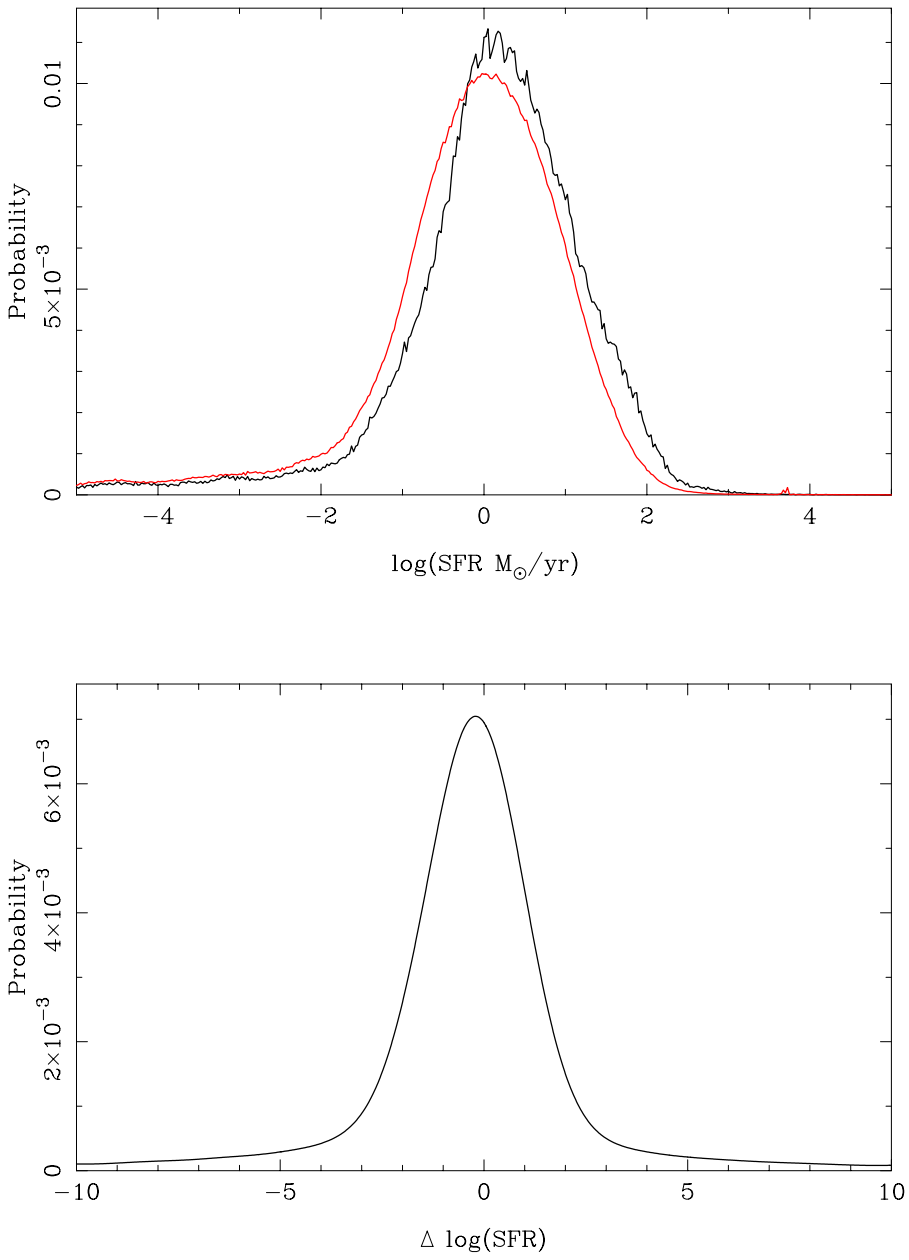

Figure 3.1: The top panel shows the super-PDF distribution for both the pair and control galaxies for the inner-most r_p bin. The pair PDF is represented by the solid black line, while the control PDF is represented by the red line. It can be seen that the two distributions are not matched to one another but rather they are offset from one another, showing that the two samples have different star formation rates. The bottom panel shows the result of the cross correlation between the pair PDF and the control PDF.

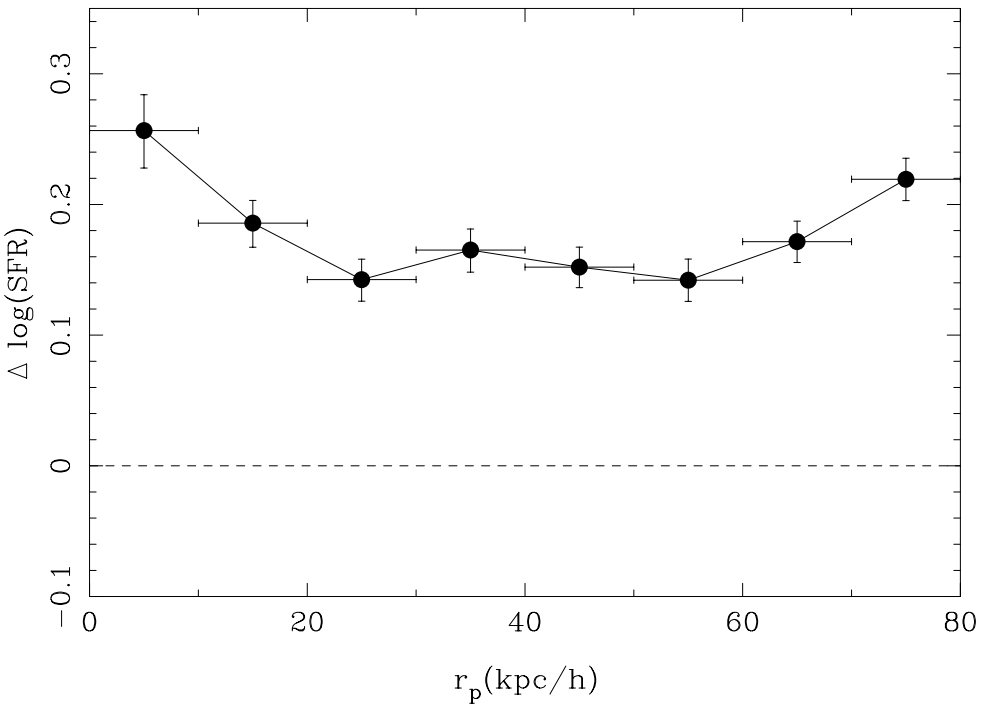

Figure 3.2: The offset found from the cross correlation of both the pair and control super PDFs for each r_p bin. There is a smooth decrease in SFR enhancement as you go from the smallest towards larger projected separations. The SFR enhancement eventually plateaus at ≈ 0.15 dex until it is further enhanced at separations of $r_p > 60$ kpc/h.

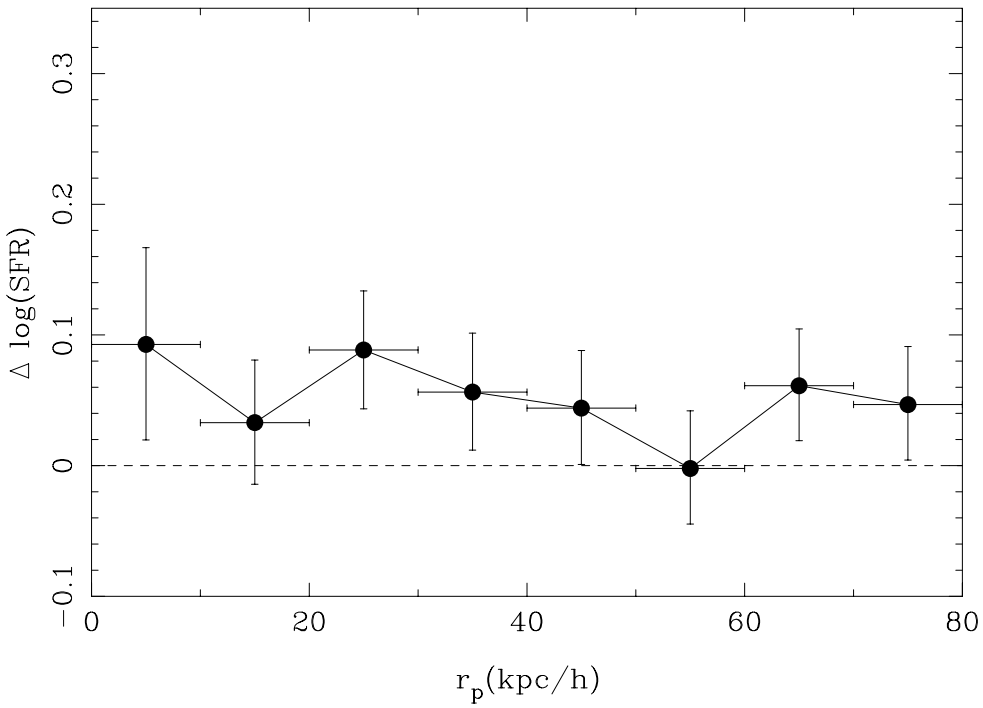

Figure 3.3: The offset found from the cross correlation of both the pair and control super PDFs for each r_p bin without any sSFR cut applied to the pairs. There is a much less significant SFR enhancement as a function of r_p when we consider all pairs galaxies.

fractions of passive and SF galaxies in the two samples. Since the full pair and control samples are dominated by red sequence galaxies, presumably the signature of constrained star formation in the PDF has been washed out.

We also have the ability to investigate whether the merger is capable of transforming a galaxy from a quiescent galaxy that will not pass our sSFR cut to a galaxy that will pass the sSFR cut as a function of pair projected separation. Figure 3.4 shows the fraction of galaxies that pass our sSFR cut as a function of r_p from the pairs sample that has no sSFR cut applied. It is shown in Figure 3.4 that there is no trend in the fraction of either the pair galaxies or their matched controls as a function of r_p by the inclusion of a sSFR cut. An interesting note on this independence on the sSFR cut is that, although there is a dependence of ΔSFR on r_p, Figure 3.4 shows that mergers do not apparently turn quiescent galaxies into star forming galaxies that pass our sSFR cut.

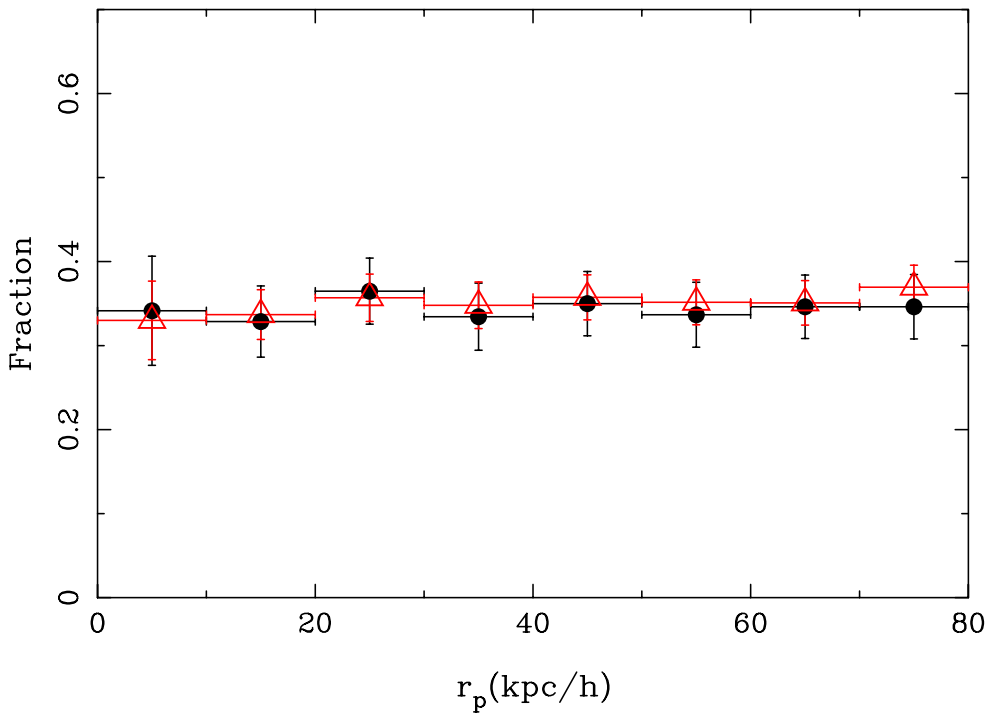

Figure 3.4: The fraction of galaxies that pass the sSFR cut as a function of the projected physical separation. This was constructed using the pairs sample that was not required to pass the sSFR cut. The pairs galaxies are shown as solid black points and the control galaxies are shown as red triangles.

3.2.1 Composite and AGN galaxies

Since broadband SED fitting does not rely on emission line diagnostics to derive a SFR, we should not be hindered in deriving the SFRs for objects that have contamination from non-stellar sources (e.g. AGN). Kauffmann et al. (2003) showed that the optical colours of galaxies are unaffected by AGN, which allows us to confidently discuss the star formation rates of these galaxies that are classified as either composite or AGN. This conclusion was reached by K03 by taking the stacked spectra of 500 galaxies classified as AGN and subtracting the stacked spectra of a stellar mass matched sample that were not classified as AGN. The residuals are presented in Figure 4 of Kauffmann et al. (2003), where it is shown that the continuum is consistent with zero; except for the added strength of some emission lines, the spectra are very similar.

We have a total of 110 close pairs galaxies that pass our sSFR cut and are classified as AGN. To these galaxies we match a total of 12 unique control galaxies per pair (1320 controls). Although this sample is considerably smaller than when considering our total pairs sample, a large number of control galaxies should help mitigate the effect of small number statistics. We also have 471 galaxies classified as composite with 15 controls matched per pair galaxy (7,065 controls). Following the same analysis as §3.1, we present the relative SFR enhancement found for AGN and composite galaxies in Figure 3.5.

Focusing first on the composite galaxies, the pair galaxies at small separations (< 50 kpc/h) are enhanced overall, but with discernable r_p trend, to a level of ≈ 0.1 dex above the control. At larger separations, there may be a hint of an increasing SFR enhancement with increasing r_p (to within the limits of the small sample).

Focusing now on the galaxies classified as AGN, we note that there is significant SFR enhancement for galaxies in the innermost r_p bin, similar to that of the total pairs sample but with more significant scatter. Beyond 20 kpc/h the enhancements scatter about the zero line; again no significant trend with r_p is observed and suggests the pair SFRs are consistent with the control.

3.3 Bulge And Disk Star Formation Enhancement

In addition to being able to study the star formation rates of interacting galaxies as a whole, we now have the information to better constrain spatially where the SFR enhancement is occurring. Using the bulge and disk decompositions described in §2.1 it is possible to separately derive physical parameters for the bulge and disk components on a galaxy by

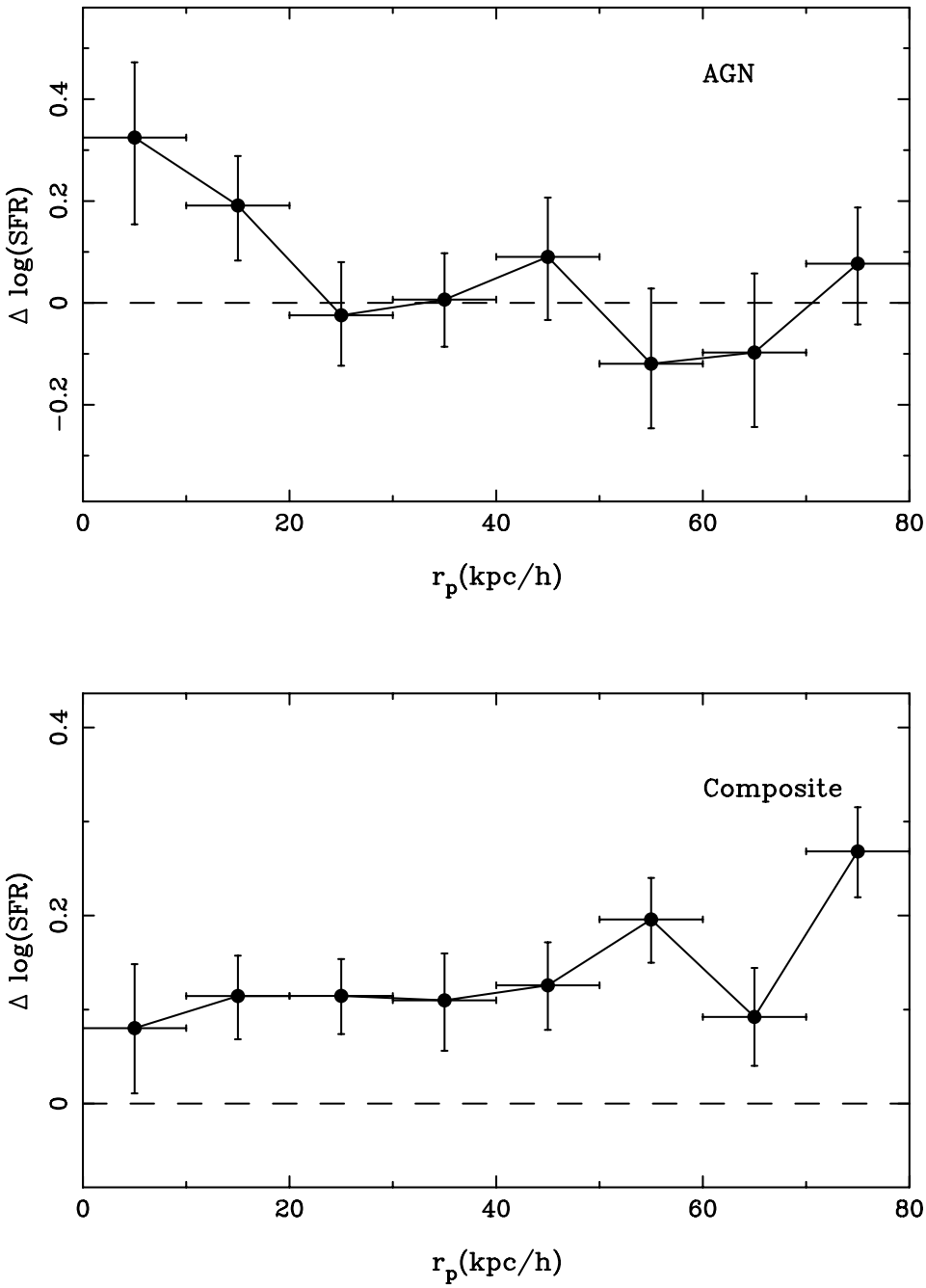

Figure 3.5: SFR enhancement as a function of projected separation found for galaxies classified as AGN or composite as defined in B04 and references therein. It can be seen that there is an overall SFR enhancement in galaxies classified as composite, but the enhancement is present only for pairs with $r_p < 20$ kpc/h when they are classified as AGN.

galaxy basis. We can therefore test whether or not the induced star formation in interacting galaxies is isolated in the central regions of the galaxy as implied by simulations (e.g. Mihos & Hernquist, 1994, 1996; Barnes & Hernquist, 1996; Cox et al., 2006; Di Matteo et al., 2007) and observationally (e.g Barton et al., 2000; Bergvall et al., 2003; Lambas et al., 2003; Alonso et al., 2004, 2006; Woods & Geller, 2007; Ellison et al., 2008, 2010; Lambas et al., 2012; Alonso et al., 2012; Scudder et al., 2012) or if it is a more diffuse process, as well as testing what kind of SFR enhancement are seen in the disks of these galaxies as well (e.g. Kennicutt et al., 1987).

A reliable bulge and disk sample is selected from the full sample of bulge and disk decompositions (§2.1). S11 define a probability, P_{pS}, which is the probability that the galaxy can be fit by a pure Sérsic profile. Following their example, we only select galaxies that have a $P_{pS} \leq 0.32$ as the one σ threshold below which they say both a bulge and disk component were needed to fit the galaxy. Requiring $P_{pS} \leq 0.32$ also ensures that the disk axial ratio distribution is flat regardless of B/T ratio, which gives confidence that these are real disks, even in bulge dominated cases.

Assuming that our sSFR cut (§ 2.10) applies to all fits done with the four SDSS bands we use (*u,g,r,i*) and our model grid, we construct a pairs sample of bulges that pass both the sSFR cut and the P_{pS} probability cut which resulted in 845 pair bulges. A control bulge sample is matched in bulge stellar mass, redshift and host galaxy environment, where we require the control bulges to pass our sSFR cut. The matching results in 5 unique controls per pair (4,225 controls) matched before the KS test failed. The same is than done for the disk component, resulting in 1,988 pair disks and 7 unique controls matched per pair disk (13,916 controls).

"Super" PDFs (§ 3.1) for both the bulge pair/control and disk pair/control components are constructed for each r_p bin. Figure 3.6 shows the SFR enhancement between pair and control bulges and disks. The red filled points show the results for the bulge component and the blue triangles are for the disk component. It can be seen that there is an enhancement in SFR for the bulge component of close pairs in the inner 30 kpc/h. The bulge SFR enhancement at larger separations is never at a value that is on par with the bulge control SFRs. At wider separations, i.e. $r_p > 50$ kpc/h, the bulge enhancement elevates again to a magnitude on par with the closest separations. The bulge enhancement is remarkably similar to the enhancement seen in the total SFR for our original pairs sample, indicating that this probably drives the overall trend in triggered star formation.

The disk component seems to paint a different picture. The disk SFR enhancement seems to be relatively flat with a median SFR enhancement at ≈ 0.1 dex. The disk en-

hancement generally occurs at a level that is below that of the bulge, suggesting that the bulge enhancement is the dominant force driving the trend seen in the total SFR enhancement. Nonetheless, this is the first time that a systematic disk SFR enhancement has been observed in a large sample of mergers.

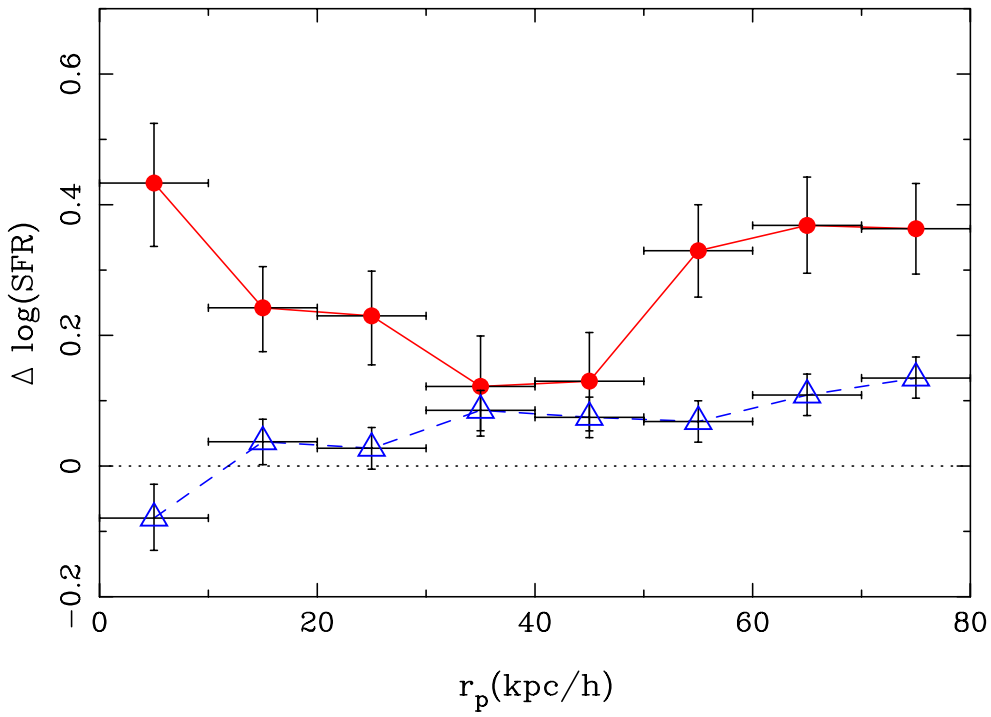

Figure 3.6: Star formation enhancement of the bulge (red filled circles) and disk (blue triangles) component of interacting galaxies. There is appreciable enhancement noted in the bulge, which is consistent with studies that use the central fibre covering as a proxy for the bulge. We also note significant enhancement at wider separations. There is also enhancement in the disk component of these interacting galaxies. However, this is always of a lesser magnitude than that of the bulge component and is correlated with r_p instead of anti-correlated. Suggesting that the majority of enhancement happens in the bulge of these interacting galaxies.

Chapter 4

Discussion

Here we discuss our results and how they fit in with the current picture of induced star formation in galaxy interactions and mergers.

4.1 Why do we pick up the upturn signature?

We want to understand the effect seen at wide separations in both our total sample and our bulge sample, i.e. that the SFR enhancement has an upturn at these wide separations, and why this has yet to be seen. To do this, we first study the exact pairs and their matched controls from Scudder et al. (2012). They extract their galaxies using strict S/N cuts to ensure that they are only dealing with galaxies that have very reliable SFRs. Scudder et al. (2012) require that a given galaxy has a S/N > 5 in Hα, Hβ, [OII]λ3727, [OIII]λ4959,5007 and [NII]λ6584 and that the ratio (Hα/Hβ) have S/N > 5. They additionally require that the galaxies be classified as star forming on the BPT diagram using the K03 line.

These strict requirements were necessary for Scudder et al. (2012) to extract galaxies that not only have a constrained SFR, but also so they can calculate a reliable gas-phase metallicity for each galaxy. See Scudder et al. (2012) and references therein for full descriptions of the gas-phase metallicity calibrations. Using these strict S/N requirements, they derive a galaxy pairs sample that has a total of 1,899 galaxy pairs. Their control matching procedure is identical to ours, matching in z, stellar mass and environment, where they match a total of 10 unique controls per pair galaxy.

The SFRs of Scudder et al. (2012) are taken directly from B04, using the SDSS spectral fits to the fibre SFRs (§ 2.8). In order to perform a similar analysis we take the SDSS fibre magnitudes and SED fit them using our model grid (§ 2.2). We compare our SED fibre

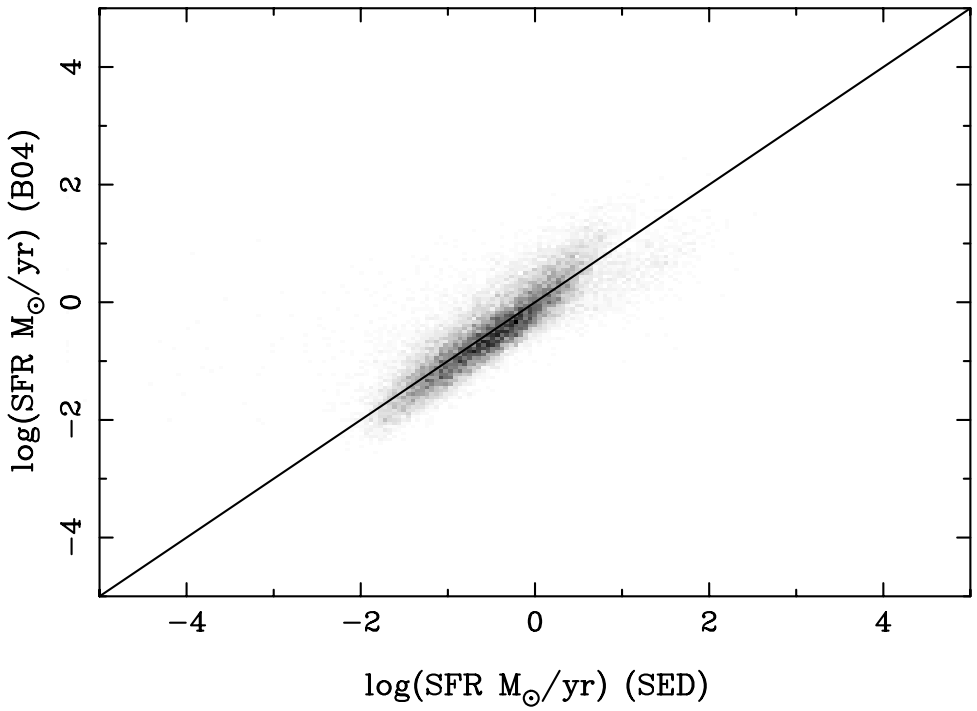

Figure 4.1: A SFR − SFR plot for the galaxies in the Scudder et al. (2012) pairs and control sample. There is good agreement between the two SFRs, with our fibre SFRs being ≈ 0.13 dex offset from B04 fibre SFRs, consistent with the offsets found in § 2.8.

SFRs to those of B04 for the Scudder et al. (2012) selected galaxies. In Figure 4.1 it can be seen that our SED fibre SFRs are in relatively good agreement with the B04 fibre SFRs. There is an ≈ 0.13 dex offset between our fibre SFRs and the B04 fibre SFRs, the offset here is consistent with the offset found when looking at the total SFRs, see § 2.8.

In Figure 4.2 we present the fibre SFR enhancements for both our SED fibre SFRs and those of Scudder et al. (2012). We show two fibre SFR enhancements using our fibre SFRs, one of which is calculated in the same manner as laid out in § 3.1 (i.e. a cross correlation of super PDFs) and the other using a method similar to Scudder et al. (2012). The Scudder et al. (2012) offsets are calculated as follows. They subtract the median SFR of each pair's control galaxies from the SFR of the pair galaxy, which gives them a distribution of Δlog(SFR) values at each r_p (see Scudder et al., 2012, Figure 2). They then bin these Δlog(SFR) values according to their projected separation and take the median value from

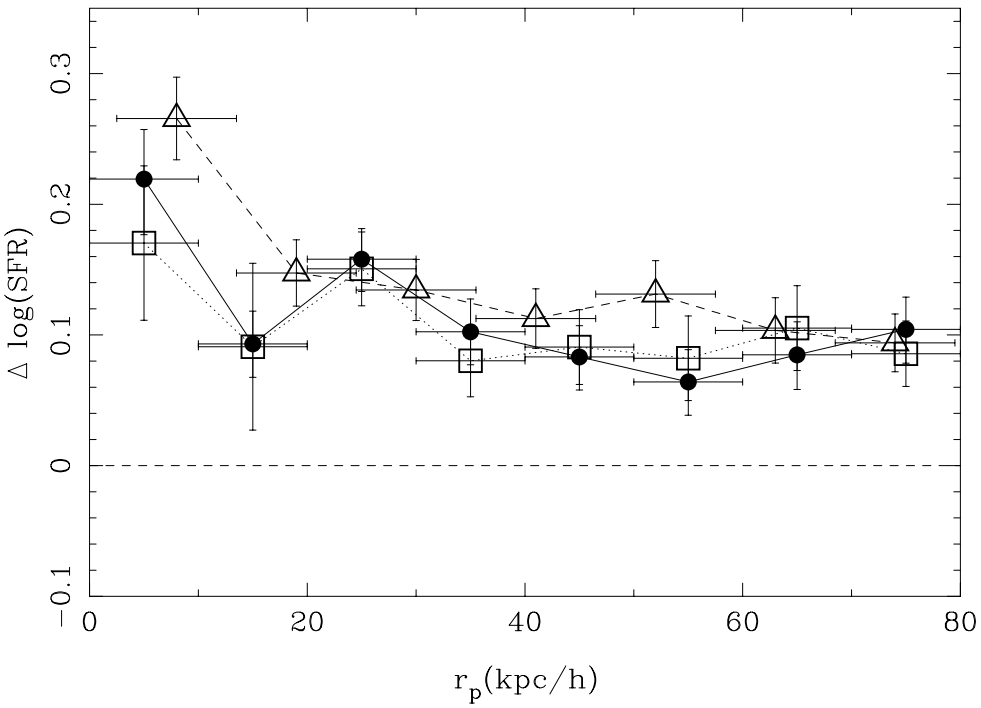

Figure 4.2: The SFR enhancement found using the pair and control samples from Scudder et al. (2012). The enhancement using our fibre SFRs and the cross correlated PDFs is shown as the solid black circles and our fibre SFRs using the Scudder et al. (2012) method as the hollow squares. The fibre SFR enhancement of Scudder et al. (2012) is shown as the hollow triangles. There is generally good agreement, within the errors, between our results.

each r_p bin as their SFR enhancement for that particular bin. Their errors for each bin come from $\sigma/\sqrt{N_{pairs}}$.

As is shown in Figure 4.2 our fibre SFR enhancements are broadly consistent with the Scudder et al. (2012) fibre SFR enhancement (hollow triangles) within the given error bars, where our fibre SFR enhancements are the solid black circles and hollow squares for the cross correlation and Scudder et al. (2012) method respectively. Since the fibre SFR enhancement seen here is consistent with the Scudder et al. (2012) sample, we can conclude that there are no biases introduced to the sample when using similar photometry, i.e. for Figure 4.2 both our study and the Scudder et al. (2012) study relied upon the SDSS fibres. We can also rule out our fitting technique and SFR enhancement method. The Scudder

et al. (2012) sample, as mentioned above, is strict in its requirements for a galaxy to be a part of the pair and control sample. We want to expand to a larger sample to test whether the upturn we observe is caused by our less stringent selection of galaxies we consider to be well constrained, where we require that galaxies pass our sSFR cut.

We look at our pairs sample that pass the sSFR cut (§ 2.11) but that are also classified as star forming by B04, which in total is 3194 pairs galaxies and we match 11 unique controls to these galaxies (35,134 control galaxies). Figure 4.3 shows the fibre SFR enhancements for these galaxies, where our SED fibre SFR enhancement is shown as solid black circles and the SFR enhancement measured from the B04 fibre SFRs is shown as the hollow squares. It can be seen that there is excellent agreement between our two measurements. We also plot the Scudder et al. (2012) fibre SFR enhancement as hollow triangles. The Scudder et al. (2012) fibre SFR enhancement values are generally below both our fibre SFR enhancements and the fibre SFR enhancement B04 would measure using our same galaxies. However, the disagreement is not concerning since the Scudder et al. (2012) galaxies have such high S/N requirements, they essentially only select the galaxies with the highest SFRs for a given mass. In turn, this selection bias effectively means that the Scudder et al. (2012) fibre SFR enhancements are a lower limit. With our sSFR cut, we do not have such a strong bias, allowing a wide range of SFRs for a given mass, resulting in our higher fibre SFR enhancements. There may be a hint of an upturn at the widest separation, however, it is only present in one bin. Therefore we conclude that our sample selection should not be the dominate factor responsible for the upturn we see at the wider separations.

We next look at the SFR enhancement we would see for the same pairs and control galaxies as Figure 4.3 but using the total SFRs instead of the fibre SFRs. In Figure 4.4 we plot our total SFR enhancement again as the solid black circles and the total SFR enhancement one would see using the B04 total SFRs as the hollow triangles. The SFR enhancement seen using our SED SFRs is very similar to that of Figure 3.2, while the SFR enhancement using the B04 total SFRs is relatively flat, with a possible decrease in SFR enhancement as you go to larger r_p. The major difference between our SED SFR enhancement and the B04 total SFR enhancement is the photometry that is used. Where our study uses the photometry provided by S11, see S11 for descriptions and references for the default SDSS extraction and how S11's determinations differ. Therefore, it is reasonable to suggest that we pick up a signature of an upturn due to the photometry being used.

Two of the major differences between the SDSS model magnitudes and the GIM2D total magnitudes are; the SDSS model magnitudes are one component fits, i.e. a galaxy is fit

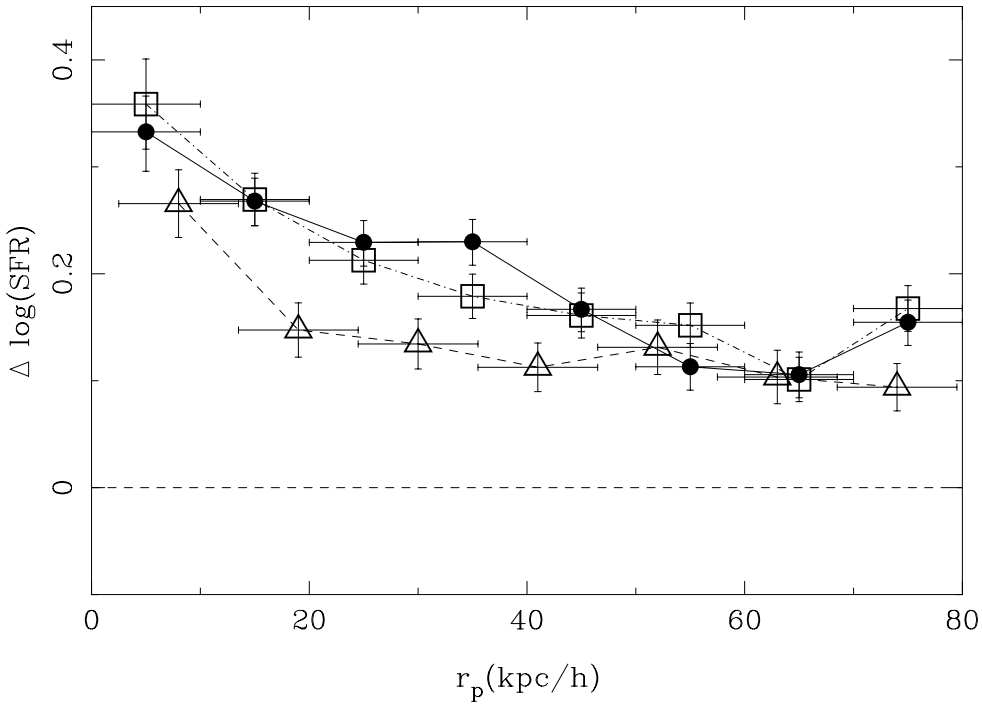

Figure 4.3: The fibre SFR enhancement found from the galaxies in our pairs sample (§ 2.11) that are classified as star forming by B04. The enhancement using our SED fibre SFRs are shown as the solid black circles and the fibre SFR enhancement that would be seen using the same galaxies but the B04 fibre SFRs are shown as the hollow squares. As can be seen there is excellent agreement between the two fibre SFR enhancements. The Scudder et al. (2012) fibre SFR enhancement are shown as the hollow triangles. The distributions are broadly consistent with one another, suggesting that our sample selection is not the dominate contributor to our measured upturn.

either by an exponential or a de Vaucouleurs profile. Galaxies with intermediate morphologies would be missing light by being restricted to this one component fit. In addition to that, the GIM2D model magnitudes are integrated to infinity. Integrating to infinity allows S11 to pick up additional flux on the outskirts of a given galaxy that could potentially contain important information. Under the assumption that the photometry provided by S11 is cleaner than the default SDSS photometry, we should consider these upturns to be a true physical phenomenon.

In brief, we have found that the SFR enhancement we measure is dependent and independent upon on several factors. We have shown that the SFR enhancement does not depend upon our the method for calculating the enhancement (Figure 4.2) or the use of SED fibre SFRs compared to the B04 fibre SFRs (Figure 4.2). We have found that the SFR enhancement does depend upon the sample selection (Figure 4.3) and also upon the photometry/aperture corrections (Figure 4.4), where the latter is suggested to be the reason we now see an upturn at wide separations.

4.2 Total integrated light

4.2.1 All galaxies

So far we have shown that there is a relative enhancement in the SFR of interacting galaxies over that of matched isolated galaxies, when both pair and control are required to pass our sSFR cut. We have shown that for the total integrated light the enhancement is a strong function of the projected physical separation, where the galaxies that are closest together have the largest enhancement. Our results are qualitatively similar to many other studies that have looked at enhanced star formation, albeit not necessarily the total SFR enhancement (e.g Barton et al., 2000; Lambas et al., 2003; Alonso et al., 2004, 2006; Woods & Geller, 2007; Ellison et al., 2008, 2010; Lambas et al., 2012; Alonso et al., 2012; Scudder et al., 2012) where they all find that the SFR for close pair galaxies is enhanced and that the magnitude of this enhancement is a strong function of the projected physical separation with increasing enhancement for decreasing separation. However, as was noted before, our SFR enhancement never reaches a value of 0 and we also observe an additional boost to the SFR of pair galaxies in our sample at wide separations.

The SFR enhancement that was shown in Figure 3.2 (§ 3.1) suggests that out to large separations the SFR of close pair galaxies does not reach down to a level that is on par with their matched controls but rather, lie on a "plateau". Previous studies have also noted

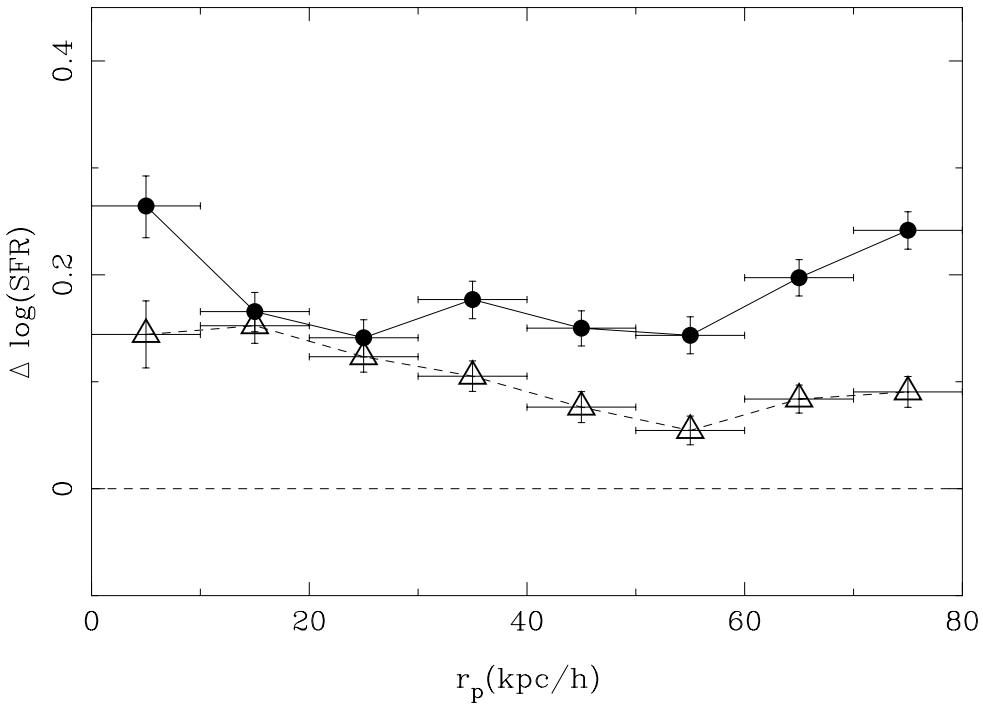

Figure 4.4: The same as Figure 4.3 except we are plotting the SFR enhancement using the total SFRs. Our total SFR enhancement values are plotted as the solid black points and the B04 total SFR enhancement values are the hollow triangles. The major difference between this figure and Figure 4.3 is the photometry that is being used to calculate the total SFRs.

a plateau at wide separations, e.g. Patton et al. (2011) when examining galaxy colours and Scudder et al. (2012), who show that the SFR enhancement as a function of projected separation is still positive and extends out to, and possibly beyond, the 80 kpc/h maximum separation that they consider. The fact that two independent studies find a plateau similar to the one observed here, gives confidence that this is a true physical phenomenon. Some explanation to a plausible cause for this plateau was given in Scudder et al. (2012), see their Figure 11, where they considered the models of Torrey et al. (2012), with slight modifications made. Scudder et al. (2012) looked at the time evolution of 16 different major mergers, varying the orbital properties between each merger. As an example they present one of the simulations where the galaxy underwent a large burst of star formation at the apocentre of its orbit and then another, larger, burst of star formation at coalescence. They note though, that the peak SFR after first passage does not necessarily have to correspond with apocentre, rather they stress there is a delay between first passage and induced star formation and that the galaxies have enough time to separate from one another. By transforming from physical separation to projected physical separation and combining their 16 simulations they were able to show that the peak in SFR at large distances is sometimes observed at smaller projected separations. The signature of enhanced star formation is therefore smeared over a larger r_p range, which results in the observed plateau of Δlog(SFR) at wide separations. Therefore, it is reasonable to assume that the plateau we observe can be attributed to a similar phenomena. The upturn that is observed is discuss in further detail in § 4.3.

4.2.2 AGN galaxies

Due to our large sample size, we are able to study specific classifications of galaxies and still have an appropriately large number for sound statistics. We can now, for the first time, address the SFR enhancement seen in galaxies classified as AGN. Our classfications are again based on the B04 classification, therefore the galaxies classified as AGN are simply galaxies that lie above the K01 line on the BPT diagram (§ 2.8). Although these galaxies are considered pure AGN galaxies, there could potentially still be significant star formation occurring in these galaxies. The enhancement we see (Figure 3.5) for AGN galaxies is qualitatively similar to other enhancements seen in previous studies (not necessarily looking at AGN) (e.g Barton et al., 2000; Lambas et al., 2003; Alonso et al., 2004, 2006; Woods & Geller, 2007; Ellison et al., 2008, 2010; Lambas et al., 2012; Alonso et al., 2012; Scudder et al., 2012), i.e. the largest enhancement at closest separations.

We note here that the significant SFR enhancement is only in the inner 20 kpc/h bins and the outer bins oscillate about zero and show no significant trend. Santini et al. (2012) found a SFR enhancement when looking at non-pair galaxies classified as AGN over a control of non-AGN galaxies, suggesting that AGN can have significant star formation. The Santini et al. (2012) sample is coarsely stellar mass and redshift matched and as was shown in Perez et al. (2009), large biases can arise from not matching in local density. As a result our control pool is slightly more stringent, and the results should be more robust.

Our results suggest that significant SFR enhancement can occur in galaxies classified as AGN. A connection between triggered star formation and AGN activity may be inferred from the works of Ellison et al. (2011) and Liu et al. (2012), where the former show that the fraction of AGN galaxies increases as a function of decreasing r_p in the same regime where SFRs are enhanced. They also noted a similar trend in galaxies classified as composites and speculate that SFR enhancement can occur concurrently in AGN as well.

The Liu et al. (2012) study looked at the Hδ absorption strength and 4000 Å break of close pairs classified as AGN, compared to stellar mass and z matched non-pair AGN. To quantify the stellar properties of their AGN they use Hδ absorption as a measure of recent starbursts and the 4000 Å break is used as a proxy for age, where young galaxies have small 4000 Å breaks compared to older populations. Liu et al. (2012) find that at separations of r_p < 10-30 kpc/h, their pair AGNs show enhanced Hδ and reduced 4000 Å strength compared to their control galaxies. Their results suggest that at close separations the AGN pairs have a younger stellar population over their matched control. Our results agree remarkably well with the Liu et al. (2012) results, in that galaxies classified as AGN have enhanced star formation at small separations (r_p < 20 kpc/h). Our results could suggest that there is a limited time that enhanced star formation can occur before processes such as AGN feedback shut it off. The view of delayed AGN activity is supported by simulations, e.g. Hopkins (2012).

4.3 Bulge and disk enhancements

In addition to studying the total SFR enhancement for galaxies, we have the opportunity to also study individual morphological components of our interacting galaxies. These morphological components will allow us to constrain spatially where the majority of SFR enhancement is occurring. We showed in Figure 3.6 that the bulge component of interacting pairs has a larger SFR relative to isolated bulges, up to a factor of 3 at the closest separations. The bulge SFR enhancement agrees well with previous studies that have noted

enhanced star formation (e.g Barton et al., 2000; Bergvall et al., 2003; Lambas et al., 2003; Alonso et al., 2004, 2006; Woods & Geller, 2007; Ellison et al., 2008, 2010; Lambas et al., 2012; Alonso et al., 2012; Scudder et al., 2012), namely that the magnitude of the SFR enhancement increases as you go towards smaller separations. The magnitude of our enhancement is larger than previous studies when potentially probing a similar region of the interacting galaxies (e.g. Ellison et al., 2008; Scudder et al., 2012), i.e. the fibre values, since it covers the central region. The fibre is generally taken as a proxy for the bulge component, whereas the bulge component we use here is an individual morphological component produced by the fits of S11 so we do not necessarily expect them to agree one to one. Significant bulge SFR enhancement is consistent with simulations of mergers. Simulations generally show that the inflowing gas during a merger primarily goes towards the central component of the galaxies, where it then fuels an intense burst of star formation (e.g. Mihos & Hernquist, 1994, 1996; Barnes & Hernquist, 1996; Cox et al., 2006; Di Matteo et al., 2007).

The bulge SFR enhancement, much like our total SFR enhancement, has a component at $r_p > 60$ kpc/h where the SFR enhancement increases again, to levels slightly below that of the closest separations. A similar upturn in SFR enhancement at large separations in the fibres was previously seen by Ellison et al. (2008). However, they partially attribute their upturn to the fact that their pairs and controls were not being matched in environment, in addition to their stellar mass and z matching. Our results should not be affected by this bias since we do our matching in z, stellar mass and environment. An upturn in the SFR enhancement at wide separations has also been noted in the suite of 16 major mergers of Scudder et al. (2012), where their simulations looked at the central regions of their mergers. Towards the largest separations they note an upturn in the SFR enhancement to a magnitude similar to the enhancement they see at the smallest separations. They caution though that their simulations are a very simplified picture of mergers and are not necessarily representative in terms of the magnitude one would expect of SFR enhancements. However, it is the idea of a delay between the interaction and the onset of star formation that is important to draw from the simulation.

The obvious next step would be to extend the study out to wider separations to test whether the enhancement continues to increase or turns back around at a later point. However, extending a close pairs sample to wide separations is a non-trivial matter. How far out can one go in projected separation until it become unfeasible to suggest two galaxies are an interacting pair? Also, as you increase the separation between pairs, you introduce an observational bias into your sample, i.e. your wide separation pairs will be biased to low

density environments. Extending our close pairs sample to a wide pairs sample is beyond the scope of this thesis. However, Patton et al. (in preparation) outline the challenges of constructing a wide pair sample and defining a robust unbiased control.

Enhanced star formation may not necessarily be isolated in the central regions during mergers. The work of Di Matteo et al. (2007) showed that there is extended enhanced star formation in their simulations of merging galaxies out to a few kiloparsecs. Kennicutt et al. (1987) also found that there was enhanced disk star formation by using the Hα EW as a tracer of the ongoing star formation. The Kennicutt et al. (1987) sample size is considerably smaller than ours, in both their interacting galaxies and controls, where they have a total of $\approx$ 100 galaxies that they consider to be interacting and $\approx$ 230 galaxies that they classify as their control group. Their control sample is not matched in z, stellar mass or environment, but rather their controls are matched in morphological type to their pairs. Our study has both more precise matching and the added advantage of numbers, 1,988 pairs galaxies with measured disk SFRs, with their 13,916 unique mass, redshift and environment matched controls needed to avoid any unnecessary biases. Our sample is then much cleaner than previous studies and should put a good constraint on disk SFR enhancement. The Kennicutt et al. (1987) study does not present their disk enhancement as a function of projected separation, rather they look only at the disk Hα EWs. For their sample as a whole, they note that the interacting disk Hα EWs are larger than their control counterparts.

Enhanced disk SFRs, although not readily noted in simulations, have been observed in observations of individual sets of interacting galaxies. Observations of some interacting galaxies have shown large bridges of gas between the two galaxies that contain numerous large HII regions which indicates ongoing star formation. An example of local interacting galaxies that have significant non-nuclear SFRs are given in Klaas et al. (2010). They studied the Antennae galaxies in detail and have noted that regions outside of both of the nuclei have a much higher SFRs than the nuclei themselves. Similar studies have been performed on selected interacting galaxies or galaxies with strong tidal features and few noted significant nuclear SFRs compared to the other components of the galaxy or galaxies (e.g. Jahan-Miri & Khosroshahi, 2001; Jarrett et al., 2006). These examples are not interpreted to be the normal disk response in galaxy interactions, rather they are a very isolated example used to illustrate possible reactions. Ours is the first study of disk SFR enhancement in a large, well constrained sample of galaxy mergers. In contrast to these studies of individual, or small local samples, at small separations (r_p < 30 kpc/h) we do not note any significant disk enhancement. However, for r_p > 30 kpc/h separation we see a relatively flat disk SFR enhancement at the level of $\approx$ 0.1 dex over the control disks. A possible ex-

planation for the lack of SFR enhancement seen in the disks at small separations could be due to an exhaustion of the available gas in the disk as they come in for their coalescence.

Overall, our results suggest that the bulge component of interacting galaxies is the primary location of induced star formation during a merger. The magnitude of this enhancement depends upon the projected separation of the merging pair, where the largest enhancement is seen at the smallest separations. We also note that there appears to be an upturn in the enhancement seen at the widest separations for both the bulge and total SFR samples, where a possible explanation to this could be due to a delay between the interaction and the onset of star formation as the gas is funnelled towards the central region. In general our results are consistent with what is found in simulations of galaxy mergers. The gas is acted upon by gravitational torques due to the changing gravitational potential of the interacting galaxies. The gas than loses angular momentum as a result of these torques and begins to funnel towards the central regions of the galaxy, where it then fuels an intense starburst. We also found that there is moderate disk enhancement as well but that this is almost always at a level that is below that of the bulge enhancement. The disk SFR enhancements are consistent with their controls for $r_p < 30$ kpc/h and overall offset for wider separations. Bournaud (2011) suggested that ISM turbulence may play a role disk SFR enhancement. ISM turbulence is not readily accounted for in simulations and can lead to non-circular motion in the galaxies available gas. This non-circular motions allows the gas to shock and collapse in extended regions of the galaxies, resulting in disk induced star formation. However, we could not find any literature on a statistical suite of simulations that include this ISM turbulence for direct comparison to our disk component. A study of disk SFRs for merging galaxies in a state of the art hydro simulation would be an interesting comparison to our observational results.

Chapter 5

Conclusions and future work

The goal of this thesis has been to develop an SED fitting code to determine SFRs of interacting galaxies. A summary of our techniques and results are given below.

A series of exponentially declining star formation histories spanning from $\log(\frac{\tau}{\mathrm{Gyr}}) = -1.5$ to -0.1 in steps of 0.2 dex and $\log(\frac{\tau}{\mathrm{Gyr}}) = 0$ to 1 in steps of 0.1 dex were constructed using the BC03 GALEX code. The models were extracted from the BC03 model spectra files and then interpolated onto a uniform log age grid. The effects of interstellar dust, determined by the Calzetti et al. (2000) dust law were applied to each model spectrum as well as the effects of cosmological redshifting using the MAKE_SED code (Sawicki & Yee, 1998; Sawicki, 2012). In total a sample of 20,685,300 individual synthetic models were produced which should cover a wide range of physical parameters that can be used to accurately describe a given galaxy.

The photometric data were taken from S11 (Simard et al., 2011). In addition to updated photometry, S11 also provide bulge and disk decompositions for each galaxy. Each of the individual components (total integrated, bulge and disk magnitudes) were SED fitted (FIT_SED, updated to include a Bayesian fitting method) using the synthetic models outlined above.

By comparing to the work of Brinchmann et al. (2004) and Kauffmann et al. (2003) we looked at the sSFR distribution of our galaxies compared to theirs. We found that in the regime where $\log(\mathrm{sSFR}/\mathrm{yr}) > -11$ our two studies are largely consistent with each other. We developed a sSFR cut to select out these well constrained galaxies.

Using these sSFR selected galaxies we constructed pairs and control samples for the total integrated light, the bulge and the disk components. Using the SFR PDFs we cross correlated the pairs with the controls to derive SFR enhancements as a function of projected separation. The main results of this thesis are as follows:

1. Our interacting galaxy pairs show a significant SFR enhancement over z, stellar mass and environment matched controls at all separations. The enhancement is ≈ 2 times the control SFR at the closest separations and plateaus to ≈ 0.15 dex; with a small rise at $r_p > 60$ kpc/h.

2. The galaxies classified to be composite do not show any strong SFR enhancement trend with r_p; rather they are wholesale offset from their control values, although there may be hints of an increase at large r_p. The galaxies classified as AGN show SFR enhancement at small separations, $r_p < 20$ kpc/h. The enhancement at the smallest separation reaches a level of ≈ 2 times over that of the control, with significant scatter compared to the total sample. Beyond $r_p > 20$ kpc/h the enhancement oscillates about the control value, resulting in no significant enhancement at these separations.

3. The bulge SFR enhancement is largest at small separations, $r_p < 30$ kpc/h, but climbs again to a similar level beyond $r_p > 60$ kpc/h, similar in shape to the total SFR enhancement. The bulge enhancement is also always elevated above that of matched controls.

4. The disk SFR enhancement is significant above the control at values of $r_p > 30$ kpc/h and broadly consistent with control SFRs below this.

5. There is no evidence in our results for galaxies to be transitioning from a passive to star forming state (as defined by our sSFR cut) as a result of mergers. We observed that the fraction of galaxies that pass our sSFR cut as a function of projected separation is flat, for both pairs and control galaxies.

Overall our results are consistent with the current view of merging galaxies, i.e. gas funnelling from the disk down to the central components of the galaxies. We have shown that the bulge has a much larger response to the merger than the disk does, as shown by the significant amount of enhanced star formation occurring in the bulge compared to the modest star formation enhancement occurring in the disk. The upturn in SFR enhancement seen in both the total integrated light and the bulge component are suggested to possibly be caused by a delay between the interaction and induced star formation.

The story does not end with fitting galaxies with either one (total integrated light) or two (bulge and disk decomposition) components. Galaxies are extended objects and the resolution of the SDSS is such that the point spread function (PSF) of the image is in

general smaller than the angular size of the galaxies. The next obvious step is to try and examine galaxies in even finer detail.

Pixel by pixel (PBP) analyses are a very useful tool for studying the spatial properties of galaxies (e.g. Abraham et al., 1999; Conti et al., 2003; Welikala et al., 2008, 2009; Welikala et al., 2011). A galaxy's individual pixels can be SED fitted with synthetic model spectra to derive the physical parameters of each pixel, such as age, stellar mass or SFR. A common assumption with PBP analysis is that each individual pixel's flux is independent of the flux of neighbouring pixels. However, this assumption is not valid if the PSF is larger than 1 pixel.

Instead of using individual pixels, under the assumption that they are spatially independent, one could select different resolution elements, defined by the size of the PSF and stack the flux from each pixel in these resolution elements to use for the fits to the synthetic model spectra. Another simpler solution, since it is not immediately clear how one would define resolution elements, would be to fit each individual pixel's flux and then convolve the final spatial map of each parameter by the PSF of the image to smooth out features that may not be physical.

Ideally with a PBP analysis we will be able to further constrain the effects that mergers have on galaxies. Our two component bulge and disk fitting revealed that the majority of enhanced star formation is occurring in the bulge component of the galaxies. However, as mentioned above a few examples of relatively local interacting galaxies that have been studied in great detail have revealed that the majority of their stars are forming not in the nuclear region but in the more extended regions, such as tidal arms. However, we cannot take these galaxies to be representative of the typical galaxy response since they are such a small subset of galaxy mergers, but we should use them as illustrative examples. By selecting a galaxy pair and control sample using the same method as described in this thesis, one could fit these interacting and isolated galaxies in a PBP manner. In a more statistical sense we could potentially study the SFR as a function of distance from the central region of the galaxy to see if any signature of enhanced star formation is picked up in the outer portions of these interacting pairs galaxies.

Bibliography

Abazajian, K. N., Adelman-McCarthy, J. K., Agüeros, M. A., Allam, S. S., Allende Prieto, C., An, D., Anderson, K. S. J., Anderson, S. F., Annis, J., Bahcall, N. A., & et al. 2009, ApJS, 182, 543

Abraham, R. G., Ellis, R. S., Fabian, A. C., Tanvir, N. R., & Glazebrook, K. 1999, MNRAS, 303, 641

Alonso, M. S., Lambas, D. G., Tissera, P., & Coldwell, G. 2007, MNRAS, 375, 1017

Alonso, M. S., Lambas, D. G., Tissera, P. B., & Coldwell, G. 2006, MNRAS, 367, 1029

Alonso, M. S., Tissera, P. B., Coldwell, G., & Lambas, D. G. 2004, MNRAS, 352, 1081

Alonso, S., Mesa, V., Padilla, N., & Lambas, D. G. 2012, A&A, 539, A46

Baldwin, J. A., Phillips, M. M., & Terlevich, R. 1981, PASP, 93, 5

Barnes, J. E., & Hernquist, L. 1996, ApJ, 471, 115

Barton, E. J., Geller, M. J., & Kenyon, S. J. 2000, ApJ, 530, 660

Bergvall, N., Laurikainen, E., & Aalto, S. 2003, A&A, 405, 31

Bertin, E., & Arnouts, S. 1996, A&AS, 117, 393

Bournaud, F. 2011, in EAS Publications Series, Vol. 51, EAS Publications Series, ed. C. Charbonnel & T. Montmerle, 107–131

Bournaud, F., Chapon, D., Teyssier, R., Powell, L. C., Elmegreen, B. G., Elmegreen, D. M., Duc, P.-A., Contini, T., Epinat, B., & Shapiro, K. L. 2011, ApJ, 730, 4

Bower, R. G., Benson, A. J., Malbon, R., Helly, J. C., Frenk, C. S., Baugh, C. M., Cole, S., & Lacey, C. G. 2006, MNRAS, 370, 645

Brinchmann, J., Charlot, S., White, S. D. M., Tremonti, C., Kauffmann, G., Heckman, T., & Brinkmann, J. 2004, MNRAS, 351, 1151

Bruzual, G., & Charlot, S. 2003, MNRAS, 344, 1000

Calzetti, D., Armus, L., Bohlin, R., Kinney, A., Koornneef, J., & Storchi-Bergmann, T. 2000, ApJ, 533, 682

Chabrier, G. 2003, PASP, 115, 763

Charlot, S., & Fall, S. M. 2000, ApJ, 539, 718

Charlot, S., & Longhetti, M. 2001, MNRAS, 323, 887

Conti, A., Connolly, A. J., Hopkins, A. M., Budavári, T., Szalay, A. S., Csabai, I., Schmidt, S. J., Adams, C., & Petrovic, N. 2003, AJ, 126, 2330

Cox, T., Jonsson, P., Primack, J. R., & Somerville, R. S. 2006, 2006 MNRAS, 373, 1013

Cox, T. J., Jonsson, P., Somerville, R. S., Primack, J. R., & Dekel, A. 2008, MNRAS, 384, 386

Di Matteo, P., Combes, F., Melchior, A.-L., & Semelin, B. 2007, A&A, 468, 61

Di Matteo, T., Springel, V., & Hernquist, L. 2005, Nature, 433, 604

Ellison, S. L., Patton, D. R., Mendel, J. T., & Scudder, J. M. 2011, MNRAS, 418, 2043

Ellison, S. L., Patton, D. R., Simard, L., & McConnachie, A. W. 2008, AJ, 135, 1877

Ellison, S. L., Patton, D. R., Simard, L., McConnachie, A. W., Baldry, I. K., & Mendel, J. T. 2010, MNRAS, 407, 1514

Hopkins, P. F. 2012, MNRAS, 420, L8

Jahan-Miri, M., & Khosroshahi, H. G. 2001, AJ, 122, 792

Jarrett, T. H., Polletta, M., Fournon, I. P., Stacey, G., Xu, K., Siana, B., Farrah, D., Berta, S., Hatziminaoglou, E., Rodighiero, G., Surace, J., Domingue, D., Shupe, D., Fang, F., Lonsdale, C., Oliver, S., Rowan-Robinson, M., Smith, G., Babbedge, T., Gonzalez-Solares, E., Masci, F., Franceschini, A., & Padgett, D. 2006, AJ, 131, 261

Kauffmann, G., Heckman, T. M., Tremonti, C., Brinchmann, J., Charlot, S., White, S. D. M., Ridgway, S. E., Brinkmann, J., Fukugita, M., Hall, P. B., Ivezić, Ž., Richards, G. T., & Schneider, D. P. 2003, MNRAS, 346, 1055

Kauffmann, G., Heckman, T. M., White, S. D., Charlot, S., Tremonti, C., Brinchmann, J., Bruzual, G., Peng, E. W., Seibert, M., Bernardi, M., Blanton, M., Brinkmann, J., Castander, F., Csabai, I., Fukugita, M., Ivezic, Z., Munn, J., Nichol, R., Padmanabhan, N., Thakar, A., Weinberg, D., & York, D. 2003, MNRAS, 341, 33

Kauffmann, G., Heckman, T. M., White, S. D. M., Charlot, S., Tremonti, C., Peng, E. W., Seibert, M., Brinkmann, J., Nichol, R. C., SubbaRao, M., & York, D. 2003, MNRAS, 341, 54

Kennicutt, Jr., R. C. 1989, ApJ, 344, 685

Kennicutt, R. J., Roettiger, K., Keel, W., van der Hulst, J., & Hummel, E. 1987, AJ, 93, 1011

Kewley, L. J., Dopita, M. A., Sutherland, R. S., Heisler, C. A., & Trevena, J. 2001, ApJ, 556, 121

Kewley, L. J., Geller, M. J., & Barton, E. J. 2006, AJ, 131, 2004

Klaas, U., Nielbock, M., Haas, M., Krause, O., & Schreiber, J. 2010, A&A, 518, L44

Lambas, D. G., Alonso, S., Mesa, V., & O'Mill, A. L. 2012, A&A, 539, A45

Lambas, D. G., Tissera, P. B., Alonso, M. S., & Coldwell, G. 2003, MNRAS, 346, 1189

Larson, R. B., & Tinsley, B. M. 1978, ApJ, 219, 46

Li, C., Kauffmann, G., Heckman, T. M., White, S. D. M., & Jing, Y. P. 2008, MNRAS, 385, 1915

Lin, L., Koo, D. C., Weiner, B. J., Chiueh, T., Coil, A. L., Lotz, J., Conselice, C. J., Willner, S. P., Smith, H. A., Guhathakurta, P., Huang, J.-S., Le Floc'h, E., Noeske, K. G., Willmer, C. N. A., Cooper, M. C., & Phillips, A. C. 2007, ApJL, 660, L51

Liu, X., Shen, Y., & Strauss, M. A. 2012, ApJ, 745, 94

Lupton, R., Gunn, J. E., Ivezic, Z., Knapp, G. R., Kent, S., & Yasuda, N. 2001, ASP Conf.Ser., 10, 269

Michel-Dansac, L., Lambas, D. G., Alonso, M. S., & Tissera, P. 2008, MNRAS, 386, L82

Mihos, J. C., & Hernquist, L. 1994, ApJL, 425, L13

—. 1996, ApJ, 464, 641

Montuori, M., Di Matteo, P., Lehnert, M. D., Combes, F., & Semelin, B. 2010, A&A, 518, A56

Oke, J. 1974, ApJS, 27, 21

Patton, D. R., & Atfield, J. E. 2008, ApJ, 685, 235

Patton, D. R., Ellison, S. L., Simard, L., McConnachie, A. W., & Mendel, J. T. 2011, MNRAS, 412, 591

Perez, J., Michel-Dansac, L., & Tissera, P. B. 2011, MNRAS, 417, 580

Perez, J., Tissera, P., & Blaizot, J. 2009, MNRAS, 397, 748

Perez, M. J., Tissera, P. B., Scannapieco, C., Lambas, D. G., & de Rossi, M. E. 2006, A&A, 459, 361

Rupke, D. S. N., Kewley, L. J., & Barnes, J. E. 2010, ApJL, 710, L156

Salim, S., Rich, R. M., Charlot, S., Brinchmann, J., Johnson, B. D., Schiminovich, D., Seibert, M., Mallery, R., Heckman, T. M., Forster, K., Friedman, P. G., Martin, D. C., Morrissey, P., Neff, S. G., Small, T., Wyder, T. K., Bianchi, L., Donas, J., Lee, Y.-W., Madore, B. F., Milliard, B., Szalay, A. S., Welsh, B. Y., & Yi, S. K. 2007, ApJS, 173, 267

Santini, P., Rosario, D. J., Shao, L., Lutz, D., Maiolino, R., Alexander, D. M., Altieri, B., Andreani, P., Aussel, H., Bauer, F. E., Berta, S., Bongiovanni, A., Brandt, W. N., Brusa, M., Cepa, J., Cimatti, A., Daddi, E., Elbaz, D., Fontana, A., Förster Schreiber, N. M., Genzel, R., Grazian, A., Le Floc'h, E., Magnelli, B., Mainieri, V., Nordon, R., Pérez Garcia, A. M., Poglitsch, A., Popesso, P., Pozzi, F., Riguccini, L., Rodighiero, G., Salvato, M., Sanchez-Portal, M., Sturm, E., Tacconi, L. J., Valtchanov, I., & Wuyts, S. 2012, A&A, 540, A109

Sawicki, M. 2012, Submitted PASP

Sawicki, M., & Yee, H. 1998, AJ, 115, 1329

Schmidt, M. 1959, ApJ, 129, 243

Scudder, J. M., Ellison, S. L., Torrey, P., Patton, D. R., & Mendel, J. T. 2012, Submitted MNRAS

Simard, L. 1998, in Astronomical Society of the Pacific Conference Series, Vol. 145, Astronomical Data Analysis Software and Systems VII, ed. R. Albrecht, R. N. Hook, & H. A. Bushouse, 108

Simard, L., Mendel, J. T., Patton, D. R., Ellison, S. L., & McConnachie, A. W. 2011, ApJS, 196, 11

Simard, L., Willmer, C. N. A., Vogt, N. P., Sarajedini, V. L., Phillips, A. C., Weiner, B. J., Koo, D. C., Im, M., Illingworth, G. D., & Faber, S. M. 2002, ApJS, 142, 1

Stasińska, G., Cid Fernandes, R., Mateus, A., Sodré, L., & Asari, N. V. 2006, MNRAS, 371, 972

Taylor, E. N., Hopkins, A. M., Baldry, I. K., Brown, M. J. I., Driver, S. P., Kelvin, L. S., Hill, D. T., Robotham, A. S. G., Bland-Hawthorn, J., Jones, D. H., Sharp, R. G., Thomas, D., Liske, J., Loveday, J., Norberg, P., Peacock, J. A., Bamford, S. P., Brough, S., Colless, M., Cameron, E., Conselice, C. J., Croom, S. M., Frenk, C. S., Gunawardhana, M., Kuijken, K., Nichol, R. C., Parkinson, H. R., Phillipps, S., Pimbblet, K. A., Popescu, C. C., Prescott, M., Sutherland, W. J., Tuffs, R. J., van Kampen, E., & Wijesinghe, D. 2011, MNRAS, 418, 1587

Tonnesen, S., & Cen, R. 2011, ArXiv e-prints

Toomre, A., & Toomre, J. 1972, ApJ, 178, 623

Torrey, P., Cox, T. J., Kewley, L., & Hernquist, L. 2012, ApJ, 746, 108

Welikala, N., Connolly, A. J., Hopkins, A. M., & Scranton, R. 2009, ApJ, 701, 994

Welikala, N., Connolly, A. J., Hopkins, A. M., Scranton, R., & Conti, A. 2008, ApJ, 677, 970

Welikala, N., Hopkins, A. M., Robertson, B. E., Connolly, A. J., Tasca, L., Koekemoer, A. M., Ilbert, O., Bardelli, S., Kneib, J.-P., & Zentner, A. R. 2011, ArXiv e-prints

White, S. D. M., & Rees, M. J. 1978, MNRAS, 183, 341

Wong, K. C., Blanton, M. R., Burles, S. M., Coil, A. L., Cool, R. J., Eisenstein, D. J., Moustakas, J., Zhu, G., & Arnouts, S. 2011, ApJ, 728, 119

Woods, D. F., & Geller, M. J. 2007, AJ, 134, 527